

This is a pre print version of the following article:

PI3K Inhibitors Curtail MYC-Dependent Mutant p53 Gain-of-Function in Head and Neck Squamous Cell Carcinoma / Ganci, F.; Pulito, C.; Valsoni, S.; Sacconi, A.; Turco, C.; Vahabi, M.; Manciocco, V.; Mazza, E. M. C.; Meens, J.; Karamboulas, C.; Nichols, A. C.; Covello, R.; Pellini, R.; Spriano, G.; Sanguineti, G.; Muti, P.; Biciato, S.; Ailles, L.; Strano, S.; Fontemaggi, G.; Blandino, G.. - In: CLINICAL CANCER RESEARCH. - ISSN 1078-0432. - 26:12(2020), pp. 2956-2971. [10.1158/1078-0432.CCR-19-2485]

*Terms of use:*

The terms and conditions for the reuse of this version of the manuscript are specified in the publishing policy. For all terms of use and more information see the publisher's website.

18/12/2025 20:03

# **PI3K inhibitors curtail MYC-dependent mutant p53 gain-of-function in head and neck squamous cell carcinoma**

Federica Ganci<sup>\*1</sup>, Claudio Pulito<sup>\*1</sup>, Sara Valsoni<sup>2</sup>, Andrea Sacconi<sup>1</sup>, Chiara Turco<sup>1</sup>, Mahrou Vahabi<sup>1</sup>, Valentina Manciocco<sup>3</sup>, Emilia Maria Cristina Mazza<sup>4</sup>, Jalna Meens<sup>5</sup>, Christina Karamboulas<sup>5</sup>, Anthony Nichols<sup>6</sup>, Raul Pellini<sup>3</sup>, Giuseppe Spriano<sup>3</sup>, Giuseppe Sanguineti<sup>7</sup>, Paola Muti<sup>8,9</sup>, Silvio Bicchato<sup>2</sup>, Laurie Ailles<sup>5</sup>, Sabrina Strano<sup>10</sup>, Giulia Fontemaggi<sup>1</sup> and Giovanni Blandino<sup>1</sup>

1. *Oncogenomic and Epigenetic Unit, IRCCS Regina Elena National Cancer Institute, 00144 Rome, Italy*
2. *Department of Life Sciences, Center for Genome Research, University of Modena and Reggio Emilia, 41125 Modena, Italy*
3. *Otolaryngology Unit, IRCCS Regina Elena National Cancer Institute, 00144 Rome, Italy*
4. *Istituto Clinico Humanitas, Rozzano, 20089, Italy*
5. *Princess Margaret Cancer Centre, University Health Network, Toronto, Ontario, Canada*
6. *Department of Otolaryngology – Head and Neck Surgery, Western University, London, Ontario, Canada*
7. *Radiotherapy Unit, IRCCS Regina Elena National Cancer Institute, 00144 Rome, Italy*
8. *Department of Oncology, Juravinski Cancer Center-McMaster University Hamilton, Ontario, Canada*
9. *School of Public Health-Harvard University, Boston, Massachusetts, USA*
10. *Molecular Chemoprevention Group, IRCCS Regina Elena National Cancer Institute, 00144 Rome, Italy*

\* These two authors contributed equally to this work.

## **E-mail addresses:**

FEDERICA GANCI: federica.ganci@ifo.gov.it  
CLAUDIO PULITO: claudio.pulito@ifo.gov.it  
SARA VALSONI: sara.valsoni@gmail.com  
ANDREA SACCONI: andrea.sacconi@ifo.gov.it  
CHIARA TURCO: turco\_chiara@icloud.com  
MAHROU VAHABI: mahrou.vahabi@gmail.com  
VALENTINA MANCIOCCO: valentina.manciocco@ifo.gov.it  
EMILIA MARIA CRISTINA MAZZA: emyemme@gmail.com  
JALNA MEENS: Jalna.Meens@uhnresearch.ca  
CHRISTINA KARAMBOULAS: Christina.Karamboulas@uhnresearch.ca  
ANTHONY NICHOLS: anthony.nichols@lhsc.on.ca  
RAUL PELLINI: Raul.Pellini@ifo.gov.it  
GIUSEPPE SPRIANO: bspriano@email.it  
GIUSEPPE SANGUINETI: Giuseppe.Sanguineti@ifo.gov.it  
PAOLA MUTI: muti@mcmaster.ca  
SILVIO BICCIATO: sbicciat@unimore.it  
LAURIE AILLES: laurie.ailles@uhnresearch.ca  
SABRINA STRANO: Sabrina.Strano@ifo.gov.it  
GIULIA FONTEMAGGI: giulia.fontemaggi@ifo.gov.it  
GIOVANNI BLANDINO: giovanni.blandino@ifo.gov.it

## **CORRESPONDING AUTHORS:**

Giovanni Blandino, M.D., Oncogenomic and Epigenetic Unit, IRCCS Regina Elena National Cancer Institute, Via Elio Chianesi, 53, 00144 Rome, Italy, Phone: +39-06-52662911;  
Fax: +39-06-52665523

Giulia Fontemaggi, PhD., Oncogenomic and Epigenetic Unit, IRCCS Regina Elena National Cancer Institute, Via Elio Chianesi, 53, 00144 Rome, Italy, Phone: +39-06-52662878;

## TRANSLATIONAL RELEVANCE

Head and neck squamous cell carcinoma (HNSCC) is typically characterized by mutation of *TP53* gene, associated to therapy resistance and high incidence of local recurrences. However, drugs specifically targeting mutant p53 proteins, frequently presenting gain-of-function activity associated with radioresistance, are not available. We then set out to identify mutant p53-associated functions that might be targeted with drugs currently used in HNSCC trials. This study identifies MYC as a crucial mediator of mutant p53 activity in HNSCC and PI3K inhibitors as compounds able to impinge on mutant p53-MYC dependent gene expression. Of note, down-regulation of mutant p53-MYC dependent genes is associated with response to PI3K $\alpha$ -selective inhibitor Alpelisib (BYL719) in HNSCC.

## **ABSTRACT**

**Background:** Mutation of *TP53* gene is a hallmark of head and neck squamous cell carcinoma (HNSCC) not yet exploited therapeutically. *TP53* mutation frequently leads to the synthesis of mutant p53 proteins with gain-of-function activity, associated with radioresistance and high incidence of local recurrences in HNSCC.

**Methods:** mutant p53-associated functions were investigated through Gene Set Enrichment Analysis in the TCGA cohort of HNSCC and in a panel of 22 HNSCC cell lines. mutant p53-dependent transcripts were analyzed in HNSCC cell line Cal27, carrying mutant p53H193L, and FaDu, carrying p53R248L. Drugs impinging on mutant p53-MYC-dependent signature were identified interrogating Connectivity Map (<https://clue.io>) derived from the Library of Integrated Network-based Cellular Signatures (LINCS) database (<http://lincs.hms.harvard.edu/>) and analyzed in HNSCC cell lines and PDX models.

**Results:** Here, we identified a signature of transcripts directly controlled by gain-of-function mutant p53 protein and prognostic in HNSCC, which is highly enriched of MYC targets. Specifically, both in patient-derived xenografts (PDX) and cell lines of HNSCC treated with the PI3K $\alpha$ -selective inhibitor BYL719 (Alpelisib) the down-regulation of mutant p53/MYC-dependent signature correlates with response to this compound. At the molecular level, mutant p53 and YAP favor the binding of MYC to its target promoters and enhance MYC protein stability. Treatment with BYL719 disrupts the interaction of MYC and mutant p53 proteins with MYC target promoters. Of note, depletion of MYC, mutant p53 or YAP potentiates the effectiveness of BYL719 treatment.

**Conclusion:** Collectively, the blocking of this transcriptional network is an important determinant for the response to BYL719 in HNSCC.

**KEYWORDS:** Head and Neck Squamous Cell Carcinoma (HNSCC), gain-of-function, p53, mutant p53, MYC, PI3K, BYL719, Alpelisib

## BACKGROUND

HNSCC comprises 5.5% of all incidence cancers and is the sixth leading cancer worldwide (1, 2). It is typically characterized by locoregional diffusion with 60% of patients affected by relapse. Unfortunately, advances in the surgical and medical treatments for HNSCC over the past two decades have not improved overall disease outcomes. As a consequence, locoregional failure is the most common cause of death in HNSCC patients (1, 2).

*TP53* is the most frequently mutated gene in head&neck squamous cell carcinomas (HNSCC) (<http://www-p53.iarc.fr>). Recently, whole-exome sequencing analyses reported that TP53 mutations occur in HNSCC with a frequency of 72% (3,4). The tetrameric transcription factor p53 is a stress responsive protein that suppresses cellular oncogenic transformation mainly by inducing growth arrest, apoptosis, senescence, DNA repair and differentiation in damaged cells (5-7). Missense mutations represent the majority of *TP53* mutations (8,9). It is becoming increasingly evident that many mutant p53 forms not only lose their tumor suppressive function but also gain new oncogenic properties (10). This notion is termed “gain-of-function” (GOF). *In vivo* and *in vitro* studies have indeed demonstrated that some mutant p53 proteins, usually expressed at markedly elevated levels in cancer cells, are associated with enhanced proliferative, invasive and angiogenic abilities (11-13). At molecular level, mutant p53 proteins exert oncogenic functions through their ability to modulate gene expression. This occurs through the interaction with other transcription factors, such as NF-Y, E2F1, NF-kB, Sp1, Ets1, SREBP-2, the Vitamin D receptor (VDR), E2F4 and YAP (14-18). An additional mechanism of gain-of-function is based on the ability of mutant p53 to bind to and sequester proteins with anti-tumor activity, such as p63 and p73 (19).

Several studies demonstrated that *TP53* status has a prognostic role in HNSCC; mutations in *TP53* indeed predict shorter overall survival, insurgence of local recurrence and cancer treatment failure (20-29).

In this study, we set out to define the transcriptional program governed by mutant p53 proteins with gain-of-function in HNSCC with the aim to highlight the most relevant mutant p53-dependent pathways that could be exploited therapeutically.

MYC emerged in our study as a major mediator of mutant p53 gain of function in HNSCC. MYC is a proto-oncogene with crucial role in tumor initiation, progression, and maintenance (30). MYC oncoproteins in solid tumors are frequently activated by copy gains but may be also induced by a variety of other mechanisms (31); importantly, it is well established that even small changes in MYC levels can drive ectopic proliferation of somatic cells and oncogenesis (32-34). MYC regulates various cancer cellular functions, including cell cycle, cell survival, proliferation and metabolic reprogramming; moreover, MYC-induced oncogenic and epigenetic reprogramming leads to the acquisition of cancer stem-like cells-associated properties and induction of the intra-tumoral heterogeneity (35).

Also during HNSCC tumorigenesis MYC plays an important role and its expression associates with poor overall survival (36, 37). Importantly, MYC depletion potentiates cisplatin-induced apoptosis in HNSCC cells (38), highlighting MYC protein as an important player in chemoresistance. Of note, it has been shown that concomitant expression of mutant p53 and MYC proteins predicts clinical outcome (DFS) in HNSCC more accurately than what these proteins do individually (39).

MYC mRNA translation, MYC protein half-life, and MYC transcriptional activity are enhanced by mitogenic signaling through receptor tyrosine kinases which activate PI3K-AKT-mTOR signaling in breast cancer (40-42). Accordingly, activation of this upstream kinase cascade is required for cell transformation by MYC in certain cellular contexts (43).

Activation of PI3K-AKT-mTOR signaling in cancer occurs as the result of activating upstream stimuli, as for example those from RTKs, or by activating mutations in components of PI3K pathway. 66% of HNSCC harbor genomic alterations in one of the major components of PI3K pathway, being *PIK3CA*, *PTEN* and *PIK3RI* the most frequently mutated genes of the pathway (44,

45). Here, we characterized the ability of PI3K inhibitors to impinge on MYC-mutant p53-dependent gene expression in HNSCC counteracting mutant p53 gain of function.

## RESULTS

### *MYC targets are enriched in mutant p53-dependent transcriptome in HNSCC*

Mutations in *TP53* gene frequently lead to the production of very stable mutant p53 proteins that may present gain-of-function (GOF) activity and induce proliferation, invasion and angiogenesis. These activities rely on the ability of GOF mutant p53 proteins to modulate gene expression through the interaction with a variety of transcription factors (11, 12). In HNSCC nearly 60% of tumors present a missense mutation in *TP53*, potentially displaying GOF activity. Here we investigated the mutant p53-associated transcriptome to highlight possible targets that could be exploited to inhibit mutant p53 oncogenic activity.

Gene Set Enrichment Analysis (GSEA) was first performed to compare HNSCC tissues carrying missense *TP53* mutation vs. wt-p53 carrying tumors. To this end, we considered 202 patients from the TCGA (The Cancer Genome Atlas) cohort of HNSCCs, adopting as inclusion criteria the absence of any chemo/radio-therapeutic treatment before surgery. The presence of a *TP53* missense mutation was significantly associated with the activation of various pathways, being EMT (Epithelial-Mesenchymal Transition), TGF-beta, MYC targets and angiogenesis the most significant (Figure 1A). A parallel GSEA analysis comparing transcriptome from HNSCC cell lines carrying *TP53* missense mutation (N=16) vs. wt-p53 cell lines (N=6) confirmed the association between the presence of missense *TP53* mutation and the activation of MYC (Figure 1B). MYC resulted as the most affected pathway also from the comparison of transcriptome obtained by RNA-seq from control Cal27 cell line, carrying endogenous mutant p53H193L, and the p53-depleted counterpart (Figure 1C-D and Supplementary Table 1). Characterization of p53H193L GOF activity in Cal27 cells is shown in Supplementary Figure 1.

On the basis of GSEA results, we analyzed tissues from a small cohort of 23 PDX models of HNSCC, with previously characterized *TP53* status (65), to evaluate if tumors with a mutated and highly expressed p53 showed any enrichment of MYC protein. As shown in Supplementary Figure 2, western blot analysis evidenced that, despite the low number of tissues with high p53 protein expression (panel A), MYC protein level was higher in tumors with highly expressed mutated p53, compared to low-p53 tumors (panel B-C). High MYC protein levels were also observed in cell lines carrying highly expressed mutant p53 protein compared to p53-null and wt-p53 carrying cell lines (Suppl. Figure 2D).

We further characterized the transcripts downregulated after p53H193L depletion in Cal27 cells, hereby indicated as mutant p53 signature (mutp53-sig), by analyzing their expression in the 202 HNSCCs from TCGA also used for the GSEA analysis. As shown in Figure 1E, mutp53-sig level is higher in tumors carrying missense *TP53* mutation, compared to wild-type *TP53* tumors. Moreover, high expression of mutp53-sig is also associated with lower probability of survival, compared to low mutp53-sig expression, as assessed by Kaplan-Meier analysis on the TCGA cohort (Figure 1F). To further characterize the activity of mutant p53 on MYC targets, we defined a mutant p53-dependent and HNSCC-specific MYC signature selecting those MYC targets of Hallmark ver.1 with a gene expression profile a) significantly correlated to MYC expression levels in two HNSCC cohorts (IRE and TCGA cohorts, see Methods) (Figure 1G), and b) modulated by mutant p53 in the RNA-seq analysis of Cal27 cells (Figure 1G). This resulted in a 22-genes MYC signature (Supplementary Table 2) that, similarly to the whole mutp53-sig, is differentially expressed between wt-p53 and mutant p53-carrying tumors (Figure 1H) and is prognostic in HNSCC (Figure 1I). Aimed at evaluating the prognostic value of the identified signatures, we first performed Univariate Cox regression analysis on the TCGA HNSCC cohort. This revealed that expression level of both mutp53-sig and 22-genes MYC signature associates with overall survival, along with *TP53* status, *TP53* copy number, and other clinical variables, as HPV status and tumor size (T) (Table 1). In a Multivariable Cox proportional hazards regression model, adjusting for the



significant prognostic factors, we determined that a high expression level of the 22-genes MYC signature predicts overall survival independently from the other variables, while mutp53-sig loses its prognostic value (Table 1). These results indicate that the 22-genes MYC-dependent signature (part of the mutp53-sig) outperforms mutp53-sig prognostic power.

**Table 1.** Univariate Cox regression analysis from TCGA HNSCC patients considering as clinical variables also mutant p53 signature (signature high) and 22-genes MYC signature (signature high), and Multivariate Cox regression analysis from TCGA HNSCC patients considering 22-genes MYC signature (signature high).

Univariate Cox regression analysis			
Variable	Hazard Ratio	Hazard ratio 95% confidence interval	P-value
Primary site oral cavity (vs. Primary site larynx)	0.7848	0.4917 - 1.2530	0.3098
Primary site pharynx (vs. Primary site larynx)	0.4248	0.1739 - 1.0380	0.0604
HPV status positive (vs. HPV status negative)	0.2865	0.1161 - 0.7074	0.00671*
Alcohol history yes (vs. Alcohol history no)	0.91005	0.5932 - 1.3960	0.666
Tobacco smoking history yes (vs. Tobacco history no)	1.7796	0.9844 - 3.2170	0.0564
Pathological N = 1 (vs. Pathological N = 0)	1.4379	0.9382 - 2.2040	0.0955
Pathological T = 3/4 (vs. Pathological T = 1/2)	1.7005	1.0880 - 2.6580	0.0198*
Histological grade G = 3/4 (vs. Histological grade G = 1/2)	0.8311	0.5185 - 1.3320	0.442
Clinical M = 1 (vs. Clinical M = 0)	3.538	0.4878 - 25.6600	0.211
TP53 status mutated (vs. TP53 status WT)	2.4598	1.4660 - 4.1280	0.000657*
TP53 copy number CNV (vs. TP53 copy number diploid)	1.6109	1.0660 - 2.4330	0.0235*
mutp53 signature high (vs. signature low)	1.8924	1.232 - 2.907	0.0036*
22-genes MYC signature high (vs. signature low)	2.2392	1.445 - 3.471	0.000312*

Multivariate Cox regression analysis			
Variable	Hazard Ratio	Hazard ratio 95% confidence interval	P-value
HPV status positive (vs. HPV status negative)	0.5247	0.1874 - 1.4690	0.2196
Pathological T = 3/4 (vs. Pathological T = 1/2)	1.5081	0.9589 - 2.3720	0.0754
TP53 status mutated (vs. TP53 status WT)	1.6164	0.8863 - 2.9480	0.1173
22-genes MYC signature high (vs. signature low)	1.7070	1.0729 - 2.7160	0.0240*
TP53 copy number CNV (vs. TP53 copy number diploid)	1.1510	0.7420 - 1.7850	0.5301

### ***Mutant p53 controls MYC target promoters in HNSCC cells***

To further verify the HNSCC specificity of the 22-genes MYC-dependent signature, we transfected Cal27 and FaDu cell lines with siRNAs directed to MYC. We confirmed that the expression of the 22-genes MYC signature decreases after the depletion of MYC (Figure 2A-B, G-H). As expected, also mutant p53 depletion led to the signature downregulation in Cal27 and FaDu cells, carrying

respectively endogenous mutant p53H193L and p53R248L with GOF (Figure 2C-D, G-H and Supplementary Figures 1 and 3).

Interestingly, also the depletion of YAP (through the use of siRNAs targeting both YAP1 and YAP2), whose targets resulted significantly enriched in GSEA analysis of mutant p53-associated transcriptomes (Figure 1A-C) and which transcriptionally cooperates with mutp53 (15, 66), impaired the expression of a subset of genes of this signature (Figure 2E-F). On the contrary, depletion of TEAD proteins, canonically considered the mediators of YAP transcriptional activity, didn't affect the expression of MYC targets (Figure 2E-F), suggesting that YAP might participate to the transcriptional control of these genes by influencing MYC activity.

Chromatin Immunoprecipitation experiments evidenced that MYC protein is recruited onto its target promoters *SF3B3*, *HPRT1* and *CCT2*, chosen as representative models, in Cal27 cells (Figure 2J). Of note, the depletion of mutant p53 or YAP decreased the interaction of MYC protein with these promoters (Figure 2I-J). Only mutant p53 protein depletion however significantly reduced the acetylation degree of histone H4 on these promoters (Figure 2K). Analysis of mutant p53 protein recruitment by ChIP analysis evidenced that also mutant p53 is recruited on these MYC target promoters in Cal27 cells and, differently from MYC, its recruitment is less affected by YAP depletion (Figure 2L).

### ***Compounds targeting the 22-genes MYC-signature sensitize HNSCC cells to conventional therapies***

As already mentioned, the presence of mutant p53 protein has been related to poor outcome in many tumors, included HNSCC, as it may favor proliferation, angiogenesis and invasion. In HNSCC, the presence of mutant p53 also associates to increased resistance to therapies and treatments failure.

As the 22-genes MYC signature robustly predicts clinical outcome in HNSCC and is highly expressed in mutant p53-expressing cells and tumor tissues, we hypothesized that the identification

of compounds, which inhibit the expression of this signature, may represent a powerful tool to counteract mutant p53-associated oncogenic functions.

To address this issue, we used the 22-genes MYC signature to interrogate Connectivity Map (<https://clue.io>) derived from the Library of Integrated Network-based Cellular Signatures (LINCS) database (<http://lincs.hms.harvard.edu/>) and containing an extensive catalogue of gene-expression profiles generated from several human cancer cells in response to more than 27,900 perturbations. This approach highlighted a number of drugs potentially able to down-regulate the 22-genes MYC signature (Supplementary Table 3). Intersecting this list with the ClinicalTrials.gov registry to identify class of compounds exploited in clinical trials for HNSCC patients led to the selection of five compounds that deserved further study (MKK-2206, PI-103, Everolimus, Fosfatinib and BMS-754807) (Figure 2M). Interestingly, all these compounds impinge on pathways that have been linked to PI3K-Akt-mTOR signaling. This has particularly intrigued us since PI3K-Akt-mTOR signaling has been extensively shown to impact on MYC activity in cancer [40-44].

We first tested the ability of these compounds to sensitize cells to conventional treatments using two HNSCC cell lines, Cal27 (carrying p53H193L) and FaDu (carrying p53R248L) cells, suitable experimental systems for drug testing as they present GOF mutant p53 proteins conferring radio-resistance (Supplementary Figures 1 and 3). We first administered increasing doses of the selected compounds and measured cell viability to identify non-toxic doses to be used in subsequent experiments for each drug (Figure 2, panels N and O). Capability of these drugs to overcome therapy resistance in HNSCC cells was then evaluated by combination treatments with conventional chemo- and radio- therapy. Specifically, cells were pre-treated with targeted agents for 24h and subsequently treated with Cisplatin-based chemotherapy or with radiotherapy. We first evaluated the effect of pre-treatment with the selected targeted drugs on the expression of the 22-genes MYC signature and evidenced that a significant decrease of these mRNAs occurs in both cell lines at the low non-toxic doses employed (Figure 2P). By measuring cell viability and colony-forming ability, we observed that MK-2206 and PI-103 synergize with radio-therapy (Supplementary Figure 4A-B-

D-E, Supplementary Figure 5A-B-D-E-G-H-J-K) and Everolimus synergizes with cisplatin treatment (Supplementary Figure 4C-F and Supplementary Figure 5C-F-I-L) in Cal27 and FaDu cells. On the contrary, MK-2206 and PI-103 didn't overcome cisplatin resistance, and Everolimus didn't overcome radioresistance, as shown in Supplementary Figure 6.

Altogether these results demonstrate that low doses of agents targeting the PI3K-Akt-mTOR signaling potentially favor the response to conventional treatments, as already indicated by the literature [reviewed in 46], and downregulate the expression of MYC-mp53-dependent genes.

### ***BYL719 as a promising therapeutic tool in HNSCC***

Our results indicate that PI3K inhibitors are compounds that should be kept in due consideration for the treatment of mutant p53-carrying HNSCC cells. Chemical development of these inhibitors has recently led to the production of a very powerful compound, the BYL719 (Alpelisib), which demonstrated effectiveness in various resistant cancers. BYL719 was designed as a specific inhibitor of PI3K $\alpha$  (47), the product of frequently mutated *PIK3CA*, and should allow for a more favorable side effect profile since it doesn't affect other components of PI3K.

Of note, BYL719 has been recently shown to be active in HNSCC (65, 67, 68) even at low doses (69) and even in tumors not carrying *PIK3CA* mutation (70).

To evaluate if BYL719 impinges on the identified 22-genes MYC signature, we first treated Cal27 and FaDu cells with increasing amounts of this drug. Western blotting analysis of phosphorylated and non-phosphorylated components of the PI3K pathway evidenced that BYL719 is active in both cell lines (Figure 3A-B). Dose-response analysis allowed us defining 5nM as the lowest dose of BYL719 able to impinge on PI3K signaling without however affecting cell viability (viability>80%) (Figure 3C-D). At this low dose we also observed significant down-regulation of the 22-genes MYC signature (Figure 3E). Combination treatments evidenced that pretreatment of cells with 5nM BYL719 also sensitized response to conventional therapies, as Cisplatin-based chemotherapy and to radio-therapy (Figure 3E-F) in both cell lines.

We next availed of PDX (patient-derived xenograft) models of HNSCC treated or not with BYL719 to evaluate whether the 22-genes MYC signature associates with response to single treatment with BYL719. Response to BYL719 treatment in this PDX cohort has been already described in detail in Ruicci et al., 2018 (65) and is summarized in Figure 4A. Analysis of the 22-genes signature expression in treated vs. untreated PDX showed a significant downregulation of the signature in tumors presenting response to this agent compared to not responsive tumors (Figure 4B). Moreover, hierarchical clustering analysis of expression values of the 22-gene signature (Treated vs. Untreated) separated responsive from not responsive tumors (Figure 4C).

***BYL719 treatment impairs recruitment of MYC and mutant p53 proteins on MYC target promoters***

To investigate possible mechanisms through which BYL719 could lead to downregulation of the 22-genes MYC signature, we performed ChIP experiments in Cal27 cells. As shown in Figure 5A, treatment with BYL719 caused the decrease in MYC protein recruitment onto its target promoters. Of note, decreased recruitment of mutant p53 protein was also observed on the same regulatory regions (Figure 5B). Concomitantly, a reduced degree of histone H4 acetylation was observed after BYL719 treatment (Figure 5C). These results suggest that BYL719 is able to disrupt the binding of the transcriptional regulators MYC and mutant p53 on these target promoters, leading to decreased transcriptional activity.

Based on these results we next evaluated whether the depletion of mutant p53 favored the response to BYL719 in HNSCC cells. As shown in Figure 5D-E, p53 interference in Cal27 and FaDu cells, carrying mutant p53, increased the response to BYL719, while no difference was observed in HN091 cells, carrying wt-p53 (Figure 5F). In Cal27 cells we assessed that also the depletion of MYC or YAP increases the response to BYL719, evaluated through a cell viability assay (Figure 5G-H). Collectively, our results show that depletion of any component of this transcriptional network potentiates BYL719-dependent effect on cell viability.

### ***Mutant p53 increases MYC protein stability upon treatment with BYL719***

To evaluate whether the decreased MYC and mutant p53 recruitment on promoters observed through ChIP assay was attributable to changes in their expression, we analyzed MYC and mutant p53 protein levels after treatment with BYL719. We observed no major changes of MYC and mutant p53 levels even at high doses of BYL719 (Figure 6A), indicating that BYL719 causes detachment of MYC and mutant p53 without affecting their overall levels. However, we interestingly observed that treatment with BYL719 decreased MYC protein level when mutant p53 expression was depleted by RNA interference in Cal27 and FaDu cells (Figure 6B-C). No MYC protein modulation was observed in HN091 cells, carrying wt-p53 (Figure 6D). In Cal27 cells we also observed MYC protein downregulation upon YAP depletion both in presence and absence of BYL719 (Figure 6E).

To investigate whether mutant p53 and YAP contribute to the stabilization of MYC protein, we evaluated the degree of ubiquitination of MYC after depletion of mutant p53 or YAP, or after treatment with BYL719. Specifically, Cal27 cells expressing a HA-tagged Ubiquitin vector were transfected with siRNAs directed to p53 or YAP, or treated with BYL719 5nM, in presence of proteasome inhibitor MG-132. Interestingly, we observed that depletion of mutant p53 or YAP leads to a striking increase of MYC ubiquitination (Figure 6F-G), while BYL719 alone doesn't affect MYC ubiquitination. Altogether these results show that treatment with BYL719 is able *per se* to disrupt MYC binding to its target promoters while in presence of reduced levels of mutant p53 (or YAP) BYL719 is also able to cause reduction of MYC protein level.

## DISCUSSION

The vast majority of HNSCCs are characterized by mutation of *TP53* gene, which is associated with decreased probability of survival. Mutations in *TP53* frequently lead to the formation of mutant proteins with gain-of-function activity positively contributing to the maintenance of malignant phenotype. We have recently shown that the presence of *TP53* mutations is particularly relevant for the outcome of advanced HNSCC (29). In this study we aimed to identify mutant p53-associated networks that could be targeted with molecular drugs currently used for HNSCC, due to the unavailability of compounds specifically targeting mutant p53 itself.

The analysis of mutant p53-associated transcriptome in HNSCC cells highlighted transcription factor MYC as a major mediator of mutant p53 activity in this experimental system. Importantly, analysis of mutant p53-associated transcriptome on the TCGA dataset of HNSCC confirmed the association between the presence of a missense mutation in *TP53* and the high expression of MYC targets, strongly generalizing the findings obtained with mutants p53H193L and p53R248L respectively in Cal27 and FaDu cell lines.

Mutant p53 had been previously shown to exert its oncogenic activity modulating gene expression through a plethora of transcriptional modulators, such as for example NF-Y and YAP (14, 15). Here, we originally show that mutant p53H193L, as well as MYC, reach the promoters of MYC target genes, modulating their expression. Interestingly, the presence of mutant p53 or YAP is also required for an efficient interaction of MYC with its binding sites. This suggests that in a mutant p53 cell context, a general increase of MYC activity could be sustained by mutant p53 protein recruitment at MYC promoters. This would represent an additional way to allow pervasive MYC hyperactivation, besides MYC gene amplification which is observed in only 14% of HNSCC and almost exclusively in HPV(-) cases. Basing on our results, mutant p53 contributes to MYC hyperactivation also by protecting MYC protein from degradation, as evidenced by the striking ubiquitination of MYC protein that is observed in the absence of mutant p53, ubiquitination that probably participates the MYC protein decrease observed in presence of treatment with BYL719.

Through the interrogation of a pharmacogenomics database we identified various classes of compounds able to potentially impact on the expression of mutant p53-MYC-dependent genes. Among other compounds, we validated the ability of PI3K/mTOR inhibitors to downregulate mutant p53-MYC-dependent genes and to sensitize HNSCC cells to conventional treatments. We particularly focused on PI3K inhibitor BYL719, designed as a specific inhibitor of PI3K $\alpha$ , the product of frequently mutated *PIK3CA* gene (47), as it is currently employed in clinical trials for HNSCC and being specific for PI3K $\alpha$  it should associate with a more favorable side effect profile (46,48). Analysis of HNSCC PDX models evidenced that downregulation of mutant p53-MYC-dependent genes correlates with response to this compound *in vivo*.

Purposely, for studies in HNSCC cells, we selected a very low dose of this compound, to avoid toxicity effects (cell viability>80%), in addition to the biological effects, and to appreciate synergy in combination treatments. At 5nM BYL719, we didn't observe any effect on cell viability but we appreciated modulation of downstream effectors as phosphor-Akt and phosphor-mTOR as well as sensitization to both radio- and chemo-therapy treatments. Moreover, at 5nM BYL719 we observed reduction of MYC and mutant p53 recruitment on MYC target promoters and parallel downregulation of mutant p53-MYC-dependent genes. Therefore, even in absence of striking effects on cell viability, a very low dose of BYL719 is able to provoke a plethora of molecular changes ranging from decreased phosphorylation of signal transducers to detachment of transcription factors from chromatin. These molecular changes (MYC and mutant p53 transcriptional inactivation) most likely create a context that allows an effective action of conventional anticancer agents. These findings support the already proposed concept of using low dose targeted drugs to sensitize to concomitant combined therapies.



Our data show that depletion of either MYC, mutant p53 or YAP significantly potentiates the response to increasing doses of BYL719, further underlining that blockage of MYC/mutant p53 activity is a prerequisite for response to BYL719. These results suggest that therapeutic approaches aimed at blocking MYC activity could strongly contribute to the efficacy of PI3K inhibitors in HNSCC. A similar scenario is present in breast cancer, where MYC amplification is associated with resistance to PI3K/mTOR inhibitors and inhibition of BRD4 antagonizes MYC-dependent resistance to PI3K inhibitors; moreover, in breast cancer cell lines derived from mutant PIK3CA-Myc double-transgenic, the BET inhibitor, JQ1, attenuates PI3K pathway reactivation after treatment with the p110 $\alpha/\delta$ -selective inhibitor, Pictilisib (49).

The crosstalk between MYC and PI3K signaling in conferring resistance to MYC- or PI3K blocking has been extensively observed in breast cancer (49) and other malignancies, and the efficacy of MYC and PI3K blocking in favoring reciprocal response to selective inhibitors supports further progression of this combination into clinical testing (50, 51).

## CONCLUSIONS

Head and neck squamous cell carcinoma (HNSCC) is typically characterized by mutation of *TP53* gene, associated to therapy resistance and high incidence of local recurrences. However, drugs specifically targeting mutant p53 proteins, frequently presenting gain-of-function activity associated with radioresistance, are not available. We then set out to identify mutant p53-associated functions that might be targeted with drugs currently used in HNSCC trials. This study identifies MYC as a crucial mediator of mutant p53 activity in HNSCC and PI3K inhibitors as compounds able to impinge on mutant p53-MYC dependent gene expression. Of note, down-regulation of mutant p53-MYC dependent genes is associated with response to PI3K $\alpha$ -selective inhibitor BYL719 (BYL719) in HNSCC.

## METHODS

### *Cell cultures and treatments*

Cal27 (mutp53H193L), FaDu (mutp53R248L) and Detroit 562 (mutp53R175H) cell lines were obtained from ATCC (Rockville, MD, USA). HN091 cells were a kind gift from Elena Di Gennaro (Istituto Nazionale Tumori - IRCCS - Fondazione G. Pascale, Napoli, Italy). These cells were cultured in RPMI-1640 (FaDu and Cal27) and DMEM (Detroit 562 and HN091) medium (Invitrogen-GIBCO, Carlsbad, CA) supplemented with 10% fetal bovine serum, penicillin (100 U/mL), and streptomycin (100 mg/mL; Invitrogen-GIBCO). All cell lines were grown at 37°C in a balanced air humidified incubator with 5% CO<sub>2</sub>.

Drug treatments: MK-2206 (Selleckchem, #S1078), Fostamatinib (Selleckchem, #S2625), BMS-754807 (Selleckchem, #S1124), PI-103 (Selleckchem, #S1038), Everolimus (RAD001) (Selleckchem, #S1120) and BYL719 (Alpelisib) (Selleckchem, #S2814), Cisplatin (Pfizer Pharmaceuticals Group, New York, USA) were dissolved according to the manufacturer's instructions. The cells were treated for 6h-24h-48h-72h-96h according to the drug and the experiment (See Results).

Irradiation treatment: The cells were plated at sub-confluent monolayer and after 24 hours they were treated with  $\gamma$ -ray irradiation from Varian Clinac 2100C source at 1, 2 and 4 Gy for 24 hours.

Combined treatments: The cells were plated at sub-confluent monolayer and after 24 hours they were pre-treated with the drug (for the doses see Results) for 6 hours and finally irradiated or treated with cisplatin at different doses for additional 24 hours before performing clonogenic or ATPlite assays.

### *Cell transfection*

The transfections were performed with Lipofectamine RNAiMax or Lipofectamine 2000 (Life Technologies, Carlsbad, California, US). All experiments were conducted according to the

manufacturer's recommendations. siRNAs were purchased from Eurofins MWG (Ebersberg, Germany) and sequences are as follows: si-SCR: 5'-AAGUUCAGCGUGUCCGGGGAG-3'; si-MYC\_1: 5'-GCCACAGCAUACAUCUGU-3'; si-MYC\_2: 5'-GGACUAUCCUGCUGCCAAG-3'; si-YAP: 5'-GACAUCUUCUGGUCAGAGA-3'; si-TEAD: 5'-CGAUUUGUAUACCGAAUAA-3'; Si-p53\_1: 5'-GACUCCAGUGGUAUAUCUAC-3' (CDS); Si-p53\_2: 5'-GGUGAACC UUAGUACC UAA-3' (3'UTR). The cells were transfected for 48-72 hours according to the cell line and the experiments (see results)

### ***RNA extraction and expression analysis***

Total RNA was extracted using the TRIZOL Reagents (GIBCO) following the manufacturer's instructions. The concentration and purity of total RNA was assessed using a Nanodrop TM1000 spectrophotometer (Nanodrop Technologies, Wilmington, DE, USA). Reverse Transcription and RT-qPCR quantification were performed respectively by MMLV RT assay and Sybr green® or Taqman Assays (Applied Biosystem, Foster City, CA, USA) according to the manufacturer's protocol. H3, GAPDH, GUSB, RPL19, RNU2 and ACTIN were used as endogenous controls to standardize gene expression. Primers and Taqman assays used are indicated in Supplementary Table 4.

For RNA sequencing analysis through NGS we extracted RNA from Cal27 cells transfected with si-SCR or si-p53 for 48h using miRNeasy kit (Qiagen, Chatsworth, CA) following the manufacturer's instructions. RNA-sequencing of total RNA from n=4 separate replicates of both TP53-silenced and control Cal27 cells has been performed on an Illumina HiSeq 2500 platform, according to the following parameters: Hiseq2500 4 plex run, 2X100 bp reads, about 60 M reads/sample (for mRNAs/lincRNAs) after preparing the libraries with the Truseq stranded with RiboZero Illumina kit.

### ***Ubiquitination assay***

A number of  $1.6 \times 10^6$  cells was transfected with a pCMV vector carrying hemagglutinin (HA)-tagged ubiquitin (Ub-HA) (52). After 18 h, cells were treated with 25  $\mu$ M MG-132 for a further 6 h. Protein extracts were immunoprecipitated as described and subjected to Western Blotting.

### ***Cell viability assay***

Manual counting and Trypan Blue dye exclusion assay were used to assess cell growth and viability were indicated. Viability of treated cells was assessed using ATPlite assay (Perkin Elmer, Massachusetts, USA) at the indicated time points, accordingly to the manufacturer's instructions. Cells ( $8 \times 10^2$  cells) were seeded in 96 well-plates and cultured for 24-48-72-96 hours (see results). Each plate was evaluated immediately on a microplate reader (Expire Technology, Perkin Elmer). Calcsyn software was used to calculate combination index (CI) (53)

### ***EnSpire® cellular label-free platform***

Cal27 and FaDu cells were seeded in specially designed 384- well plate with highly precise optical sensors able to measure changes in light refraction resulting from dynamic mass redistribution (DMR) within the cell's monolayer. Change in the light refraction was indicated by a shift in wavelength.

### ***Lysate preparation and immunoblotting analysis***

Cells were lysed in buffer with 50 mM Tris-HCl pH 8, with 1% NP-40 (IgepalAC-630) 150 mM NaCl, 5 mM EDTA and fresh protease inhibitors. Extracts were sonicated for 10 s and centrifuged at 12000× rpm for 10 min to remove cell debris. Protein concentrations were determined by colorimetric assay (Bio-Rad). In the co-immunoprecipitation the lysis buffer was modified accordingly the protein isoelectric point. Protein concentrations were determined by colorimetric assay (Bio-Rad, Hercules, CA, USA). For each immunoprecipitation, 1  $\mu$ g of rabbit c-Myc (Cell Signaling, #5605) and 1  $\mu$ g of rabbit IgG (Santa Cruz Biotech, sc66931) as control were used.

Precleared extracts were incubated with protein A/G-Agarose beads (Thermo Fisher Scientific, Rockford, IL, USA) in lysis buffer containing 0.05% BSA and antibodies, under constant shaking at 4°C for 3 hrs. After incubation, agarose bead-bound immunocomplexes were rinsed with lysis buffer and eluted in 50 ml of SDS sample buffer for western blotting. The following primary antibodies were used: anti-c-Myc (Santa Cruz, sc-40); anti-p53(Santa Cruz, sc-6243); anti-phospho Akt (ser473) (Cell Signaling, #4058); anti-Akt (Cell Signaling, #4685); anti-phospho-mTOR (Ser-2448) (Cell Signaling, #2971); anti-mTOR (Cell Signaling, #4685); anti- GAPDH (Santa Cruz, sc-32233); anti-phospho p70 S6 Kinase (thr389) (Cell Signaling, #9234); anti-p70 S6 (Cell Signaling, #9202); anti S6 (Cell Signaling, #2317); anti-phospho S6 (ser235/236) (Cell Signaling, #2211); anti-HA (Santa Cruz, sc-57592). Secondary antibodies used were goat anti-mouse and goat anti-rabbit, conjugated to horseradish peroxidase (Amersham Biosciences,Piscataway, NJ). Immunostained bands were detected by chemiluminescent method (Pierce, Rockford, IL).

### ***Wound healing assay***

Cells seeded in 6-well tissue culture and grown to 95% confluence wounded with a sterile 10- $\mu$ L pipet tip to remove cells by one perpendicular line. PBS1x washing was used to remove loosely attached cells. Digital micrographs were taken after scratching at the indicated times.

### ***Transwell migration assay***

Migration assay was performed using a 24-well plate with a non-coated 8-mm pore size filter in the insert chamber (Falcon). Cells were transfected with siRNA-SCR as negative control or siRNA-p53 (Eurofins genomics). 48 hours after transfection, HNSCC cells were resuspended in RPMI media with 1% FBS and seeded into the insert chamber. Cal 27 cells were allowed to migrate for 48 hours or 72 hours into the bottom chamber containing 0.7 ml RPMI media containing 10% FBS in a humidified incubator at 37°C in 5% CO<sub>2</sub>. Migrated cells that attached to the outside of the filter were visualized by staining with DAPI and counted.

### ***Clonogenic assays***

Cal 27 and FaDu cell lines were grown to 70% confluence and pulse treated with the indicated drugs or transfected with siRNA. 48hrs after transfection or 16hrs later, cells were detached and seeded at 500-1500 cells/well into 6-well dishes (COSTAR) in drug-free media. Fresh media (25%) was added every five days. Colonies were stained with crystal violet and colonies (>50 cells) counted after 10- 14 days.

### ***ChIP Analysis***

Chromatin Immunoprecipitation was performed as previously reported (Di Agostino 2006). Mouse monoclonal anti-MYC (Santa Cruz, sc-40), anti-p53 (Santa Cruz, DO1, sc-126) and anti-H4 pan-acetylated (Millipore, 06-598) were used for immunoprecipitations. Cal27 cells at <50% confluence were either treated with 5nM BYL719 for 24h or transfected with siRNAs directed to p53 or YAP (sequences listed above) for 48h before crosslinking with 1% formaldehyde. SF3B3, CCT2 and HPRT1 promoters were amplified using the primer pairs included in Supplementary Table 4.

### ***PDX models of HNSCC***

All animal experiments were performed with the approval of the University Health Network Animal Care Committee (protocol #1542) and adhered to the Canadian Council on Animal Care guidelines. Fresh surgical HNSCC specimens were received from consenting patients within 0.5 to 24 hours of surgery under a University Health Network Research Ethics Board approved protocol (REB# 12-5639). PDX models were established by implanting small tissue fragments (~1mm<sup>3</sup>) under the skin on the flanks of NOD/SCID/IL2R $\gamma$ <sup>-/-</sup> (NSG) mice. Once tumors reached 1–1.5 cm in diameter mice were euthanized and tumors were dissociated in Media199 containing 1X collagenase/hyaluronidase (Stem Cell Technologies) and DNASE 1 (125 U/mL; Worthington) and injected subcutaneously into 4 mice per tumor model (minimum 100,000 cells/mouse) in 1:1

Matrigel/PBS. When tumor volumes reached 80–120 mm<sup>3</sup> mice were randomized into BYL719 treatment (Novartis; 50mg/kg) and vehicle control (corn oil) groups and treated by oral gavage 5 days/week. Mice were evaluated for tumor size and body weight every 2–4 days. Individual tumor volumes were calculated by the formula: [length x (width)<sup>2</sup>] x 0.52. A PDX model was considered responsive to BYL719 treatment if they had a statistically significant growth delay (a significant difference in slopes of growth curves using mixed model regression on repeated measures).

***PDX response calls.*** The response of PDXs to BYL719 was determined by comparing the mean tumor volume change at time t to its baseline size: % tumor volume change =  $\Delta V_t = 100\% \times ((V_t - V_{\text{initial}})/V_{\text{initial}})$ . Specifically, we determined the ‘Best Average Response’ (BestAvgResponse) by calculating the average of  $\Delta V_t$  from t = 0 to t, for each time point and then taking the minimum average found, where t > 10 days. This metric uniquely captures the durability and strength of response (Gao et al., 2015). To categorize responses, we used the modified RECIST (mRECIST) criteria established by Gao et al., which is based on the Response Evaluation Criteria in Solid Tumors (RECIST)—a set of clinically-established criteria defining when cancer patients “respond”, remain unchanged (“stable”) or “progress” during the course of their treatment (Therasse et al., 2000). The mRECIST criteria considers both the BestAvgResponse, described above, as well as the ‘Best Response’ (BestResponse) which is the minimum value of  $\Delta V_t$  for t > 10 (Gao et al., 2015). All models included in our PCT received a minimum of 14 days of treatment with BYL719.

### ***Bioinformatics analysis of Cal27 RNA-seq data***

Reads from Cal27 RNA-seq were quality controlled using FastQC (<http://www.bioinformatics.babraham.ac.uk/projects/fastqc>) and trimmed using Trimmomatic v0.32 (54). Remaining paired reads were aligned to the human genome using TopHat2 (55-56) and UCSC assembly (version hg19) and Gencode (version 19, GRCh37, Ensemble releases 74, 75) as reference genome and transcriptome, respectively. From the GTF file we excluded some annotation features (pseudogenes, mitochondrial and ribosomal RNAs, small RNA, immunoglobulin coding

genes) and retained only genes annotated as “known”. Expression levels were quantified using *HTSeq* (57) with the “union mode” after sorting reads by name with *samtools* (58). Differential expression analysis was conducted with *edgeR* (59) after filtering genes with low expression level ( $< 1$  count per million (cpm) in at least half of the samples) and considering samples as paired. Differentially expressed genes (DEGs) were identified setting the false discovery rate (FDR) threshold to 0.05 (Supplementary Table 1). Global unsupervised clustering was performed using the function *hclust* of R stats package with Pearson correlation as distance metric and average agglomeration method. Gene expression heatmaps have been generated using the function *heatmap.2* of R *gplots* package after row-wise standardization of the expression values.

### ***Analysis of HNSCC tumor cohorts***

We downloaded gene expression data (raw counts and RSEM), mutations, and clinical information of the HNSCC TCGA cohort from Firehose Broad Genome Data Analysis Centre (GDAC; <https://gdac.broadinstitute.org/>). LOH and processed copy number variation (CNV) of the TP53 gene data were downloaded from Synapse and cBioPortal databases, respectively. Out of the original samples of the TCGA-HNSCC dataset, we selected only the 202 primary tumors that had a single annotated mutation of TP53 (wt and missense, non-sense, frame-shift mutation) and that received no neoadjuvant treatment. Raw counts were normalized, and gene expression levels quantified as counts per million (cpm) using functions of the *edgeR* R package.

Gene expression data of the IRE cohort (n=22) were generated from raw .CEL files. Briefly, Probe level signals were converted to expression values using robust multi-array average procedure (RMA) (60) of Bioconductor *affy* package and a custom definition file for human Gene 1.0 ST arrays based on Entrez genes from BrainArray ([http://brainarray.mbni.med.umich.edu/Brainarray/Database/CustomCDF/CDF\\_download.asp](http://brainarray.mbni.med.umich.edu/Brainarray/Database/CustomCDF/CDF_download.asp); hugene10sthsentrezgcdf version 17.1.0). All analyses were performed in R environment version 3.0.1 using BioC version 2.12 and Bioconductor packages.



Average signature (gene set) expression has been calculated as the standardized average expression of all signature genes in sample subgroups (e.g. P53 mutant, P53 WT).

To identify two groups of tumors with either high or low mutp53-sig and 22-gene MYC signature, we used the classifier described in (61), i.e., a classification rule based on the signature score. Tumors were classified as signature ‘Low’ or signature ‘High’ if the combined score was negative or positive, respectively. This classification was applied to expression values of the TCGA cohort. To evaluate the prognostic value of the mutp53-sig and 22-gene MYC signatures, we estimated, using the Kaplan–Meier method, the probabilities of patient overall survival. Kaplan–Meier curves were compared using the log-rank (Mantel–Cox) test. P-values were calculated according to the standard normal asymptotic distribution. Survival analysis was performed in GraphPad Prism.

### ***Gene Set Enrichment Analysis***

Functional over-representation was performed using Gene Set Enrichment Analysis (GSEA; <http://software.broadinstitute.org/gsea/index.jsp>) (62), the curated gene sets of the Molecular Signatures Database (MSigDB) (63) derived from the Hallmark and Biocarta collections (<http://software.broadinstitute.org/gsea/msigdb/collections.jsp>) and the gene sets listed in (64). For Cal27 and TCGA-HNSC RNA-seq data, GSEA was run in *preranked* mode using the log2 fold change of all genes. Gene sets were considered significantly enriched at false discovery rate (FDR)  $\leq 0.25$  when using *classic* as metric and 1.000 permutations. The dot plot, showing the most significantly enriched gene sets in si-mutp53 Cal27 cells in missense P53 TCGA-HNSC tumors and a panel of missense HNSCC cell lines (E-MTAB-3610) (71) was generated using the *ggplot* function of the *ggplot2* R package.

### ***Identification of a mt-p53-myc-dependent HNSCC signature***

We defined the 22-genes mutant p53-dependent and HNSCC-specific MYC signature selecting those MYC targets of the Hallmark collection (HALLMARK\_MYC\_TARGETS\_V1) with a gene

expression profile a) significantly correlated to MYC expression levels in the TCGA and IRE HNSCC cohorts, and b) modulated by mutant p53 in the RNA-seq analysis of Cal27 cells. Briefly, the HALLMARK\_MYC\_TARGETS\_V1 gene set was first merged to gene sets of the Biocarta collection and used as input in the GSEA analysis together with the expression profile of MYC gene in the TCGA and IRE HNSCC tumors as continuous phenotype label. We then selected the core enrichment gene lists from the 2 analyses, obtaining two lists of MYC targets significantly correlated with the MYC mRNA profile in the tumor samples. Merging these two lists (n= 111 and n=108 genes using TCGA and IRE samples, respectively), we obtained a combined list of 81 genes. Finally, we intersected these 81 genes with the 1498 down-regulated genes obtained from the si-p53 vs. scr comparison on Cal27 cells and generated the 22-genes mt-p53- and myc- dependent signature (Supplementary Table 2).

### ***Identification of potential inhibitor of mt-p53-myc-dependent HNSCC activity signature***

The mt-p53-MYC- dependent signature was used to interrogate the Library of Integrated Network-based Cellular Signatures (LINCS; <http://www.lincsproject.org/>) through Connectivity Map (data version 1.1.1.2 and software version 1.1.1.38; <https://clue.io/>) to identify compounds whose administration to cancer cells results an opposite expression profile of the 22-gene signature. Briefly, Connectivity Map generates a list of compounds rank-ordered by the similarity of differentially-expressed genes in treated cells to the query gene signature and characterized by a score that ranges from -100 to 100 (based on the overlap with up- or down-regulated genes after the perturbation and the strength of the enrichment). In particular, a negative score indicates that the compound and the query signatures are opposing, i.e. genes of query signature are decreased by treatment with the compound. The magnitude of the score corresponds to the magnitude of similarity or dissimilarity. Drugs with negative score (i.e. drugs that revert the signature expression levels) were filtered retaining those with a score lower than the 90th percentile of all scores (-97.6).

Among the 243 resulting compounds, we used the ClinicalTrials.gov registry to further select 5 drugs already in clinical trial for the treatment of HNSCC tumors.

## **LIST OF ABBREVIATIONS**

HNSCC: head and neck squamous cell carcinoma

PDX: patient-derived xenografts

LINCS: Library of Integrated Network-based Cellular Signatures

GOF: gain-of-function

PI3K: phosphatidylinositol-3 kinase

TCGA: The Cancer Genome Atlas

GSEA: Gene Set Enrichment Analysis

IRE: IRCCS Regina Elena National Cancer Institute, Rome, Italy

mp53: mutant p53

wt-p53: wild-type p53

siRNAs: small-interfering RNAs

BYL719: Alpelisib

## **DECLARATIONS:**

### ***Ethics approval and consent to participate***

The study involved patients with histologically confirmed primary head and neck squamous cell carcinoma (HNSCC) undergoing curative treatment at the Otolaryngology Head and Neck Surgery Department of IRCCS Regina Elena National Cancer Institute (IRE, Rome). Enrollment of these patients has been approved by the scientific ethic committee of IRE (Rome) (protocols CE/379/08 and CE/868/16).

### ***Availability of data and material***

The TCGA dataset analysed during the current study was obtained from the Genome Data Analysis Centre (GDAC) repository (<https://gdac.broadinstitute.org/>). Cal27 RNA-seq raw data are available upon request. Affymetrix gene expression raw data of HNSCC tumors and normal counterparts from the IRE cohort are available in GEO database (GSE107591).

### ***Competing interests***

The authors declare that they have no competing interests

### ***Funding***

The research leading to these results has received funding from AIRC under IG 2017 - ID. 20613 project – P.I. Blandino Giovanni and from MIUR Epigen (13/05/R/42) – P.I. Blandino Giovanni;

### ***Authors' contributions***

F.G., C.P., G.F., S.S., G.B. conceived the study, designed the experiments and interpreted the data; S.V., A.S., E.M., S.B., performed computational and statistical data analysis; F.G., C.P., G.F., C.T., M.V., performed the cellular and molecular biology studies; J.M., C.K., A.N., L.A., performed the in vivo experiments with PDX HNSCC models; V.M., R.P., G.S., G.S., collected HNSCC samples from IRE cohort and relative clinical information; P.M., S.B. reviewed critically the work. G.F., and G.B. wrote the manuscript.

### ***Acknowledgements***

Not applicable

## REFERENCES

1. Leemans CR, Braakhuis BJ, Brakenhoff RH. The molecular biology of head and neck cancer. *Nat Rev Cancer* 2011;11:9-22.
2. Ganci F, Sacconi A, Manciocco V, Spriano G, Fontemaggi G, Blandino G. Radioresistance in Head and Neck Squamous Cell Carcinoma: Possible Molecular Markers for Local Recurrence and New Putative Therapeutic Strategies. In: Marcu LG, editor. *Contemporary Issues in Head and Neck Cancer Management*. 2015; 3-34.
3. Stransky N, Egloff AM, Tward AD, Kostic AD, Cibulskis K, Sivachenko A, et al. The mutational landscape of head and neck squamous cell carcinoma. *Science* 2011;333:1157-1160.
4. Cancer Genome Atlas Network. Comprehensive genomic characterization of head and neck squamous cell carcinomas. *Nature* 2015; 517:576-82.
5. Kasthuber ER, Lowe SW. Putting p53 in Context. *Cell* 2017;170(6):1062-78 doi 10.1016/j.cell.2017.08.028.
6. Laptenko O, Prives C. Transcriptional regulation by p53: one protein, many possibilities. *Cell Death Differ* 2006;13(6):951-61 doi 10.1038/sj.cdd.4401916
7. Kastan MB, Onyekwere O, Sidransky D, Vogelstein B, Craig RW. Participation of p53 protein in the cellular response to DNA damage. *Cancer Res* 1991;51(23 Pt 1):6304-11.
8. Olivier M, Hollstein M, Hainaut P. TP53 mutations in human cancers: origins, consequences, and clinical use. *Cold Spring Harb Perspect Biol* 2010;2(1):a001008 doi 10.1101/cshperspect.a001008.
9. Muller PA, Vousden KH. p53 mutations in cancer. *Nature Cell Biology* 2013;15: 2-8.
10. Oren M, Rotter V. Mutant p53 gain-of-function in cancer. *Cold Spring Harbor perspectives in biology* 2010;2(2):a001107.
11. Freed-Pastor WA, Prives C. Mutant p53: one name, many proteins. *Genes & development* 2012;26(12):1268-86.
12. Strano S, Dell'Orso S, Di Agostino S et al. Mutant p53: an oncogenic transcription factor. *Oncogene* 2007; 26: 2212-2219.
13. Olive KP, Tuveson DA, Ruhe ZC, Yin B, Willis NA, Bronson RT, et al. Mutant p53 gain of function in two mouse models of Li-Fraumeni syndrome. *Cell* 2004;119(6):847-60 doi 10.1016/j.cell.2004.11.004.
14. Di Agostino S, Strano S, Emiliozzi V et al. Gain of function of mutant p53: the mutant p53/NF-Y protein complex reveals an aberrant transcriptional mechanism of cell cycle regulation. *Cancer Cell* 2006; 10: 191-202.
15. Di Agostino S, Sorrentino G, Ingallina E, Valenti F, Ferraiuolo M, Biciato S, Piazza S, Strano S, Del Sal G, Blandino G. YAP enhances the pro-proliferative transcriptional activity of mutant p53 proteins. *EMBO Rep*. 2016 Feb;17(2):188-201.
16. Fontemaggi G, Dell'Orso S, Triscioglio D, Shay T, Melucci E, Fazi F, Terrenato I, Mottolese M, Muti P, Domany E, et al. 2009. The execution of the transcriptional axis mutant p53, E2F1 and ID4 promotes tumor neo-angiogenesis. *Nature Structural & Molecular Biology* 16: 1086-1093.
17. Stambolsky P, Tabach Y, Fontemaggi G, Weisz L, Maor-Aloni R, Siegfried Z, Shiff I, Kogan I, Shay M, Kalo E, Blandino G, Simon I, Oren M, Rotter V. Modulation of the vitamin D3 response by cancer-associated mutant p53. *Cancer Cell*. 2010 Mar 16;17(3):273-85.
18. Weisz L, Damalas A, Lontos M, Karakaidos P, Fontemaggi G, Maor-Aloni R, Kalis M, Levrero M, Strano S, Gorgoulis VG, Rotter V, Blandino G, Oren M. Mutant p53 enhances nuclear factor kappaB activation by tumor necrosis factor alpha in cancer cells. *Cancer Res*. 2007 Mar 15;67(6):2396-401.
19. Strano et al., 2002 Physical Interaction with Human Tumor-derived p53 Mutants Inhibits p63 Activities
20. Poeta ML, Manola J, Goldwasser MA et al. TP53 mutations and survival in squamous-cell carcinoma of the head and neck. *N Engl J Med* 2007; 357: 2552-2561.
21. Gross AM, Orosco RK, Shen JP, Egloff AM, Carter H, Hofree M, et al. Multi-tiered genomic analysis of head and neck cancer ties TP53 mutation to 3p loss. *Nature genetics* 2014;46(9):939-43.
22. Neskey DM, Osman AA, Ow TJ, Katsonis P, McDonald T, Hicks SC, et al. Evolutionary Action Score of TP53 Identifies High-Risk Mutations Associated with Decreased Survival and Increased Distant Metastases in Head and Neck Cancer. *Cancer research* 2015;75(7):1527-36.

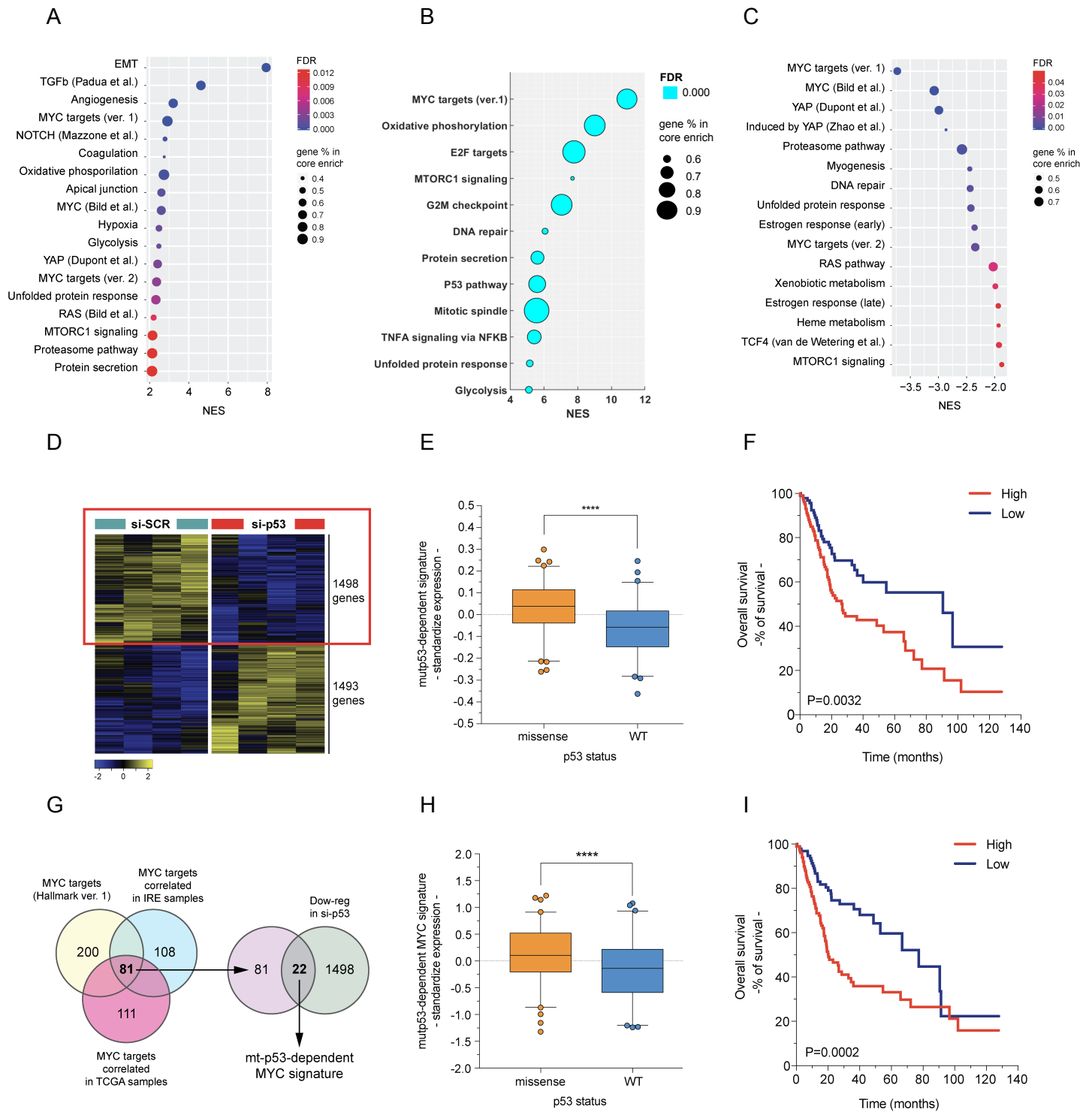
23. Peltonen JK, Vahakangas KH, Helppi HM, Bloigu R, Paakko P, Turpeenniemi-Hujanen T. Specific TP53 mutations predict aggressive phenotype in head and neck squamous cell carcinoma: a retrospective archival study. *Head & neck oncology* 2011;3:20.
24. Thomas GR, Nadiminti H, Regalado J. Molecular predictors of clinical outcome in patients with head and neck squamous cell carcinoma. *Int J Exp Pathol* 2005; 86: 347-363.
25. Erber R, Conradt C, Homann N et al. TP53 DNA contact mutations are selectively associated with allelic loss and have a strong clinical impact in head and neck cancer. *Oncogene* 1998; 16: 1671-1679.
26. Peltonen JK, Vahakangas KH, Helppi HM et al. Specific TP53 mutations predict aggressive phenotype in head and neck squamous cell carcinoma: a retrospective archival study. *Head Neck Oncol* 2011; 3: 20.
27. Lindenberg-van der Plas M, Brakenhoff RH, Kuik DJ et al. Prognostic significance of truncating TP53 mutations in head and neck squamous cell carcinoma. *Clin Cancer Res* 2011; 17: 3733-3741.
28. Skinner HD, Sandulache VC, Ow TJ et al. TP53 disruptive mutations lead to head and neck cancer treatment failure through inhibition of radiation-induced senescence. *Clin Cancer Res* 2012; 18: 290-300.
29. Ganci F, Sacconi A, Bossel Ben-Moshe N, Manciocco V, Sperduti I, Strigari L, et al. Expression of TP53 mutation-associated microRNAs predicts clinical outcome in head and neck squamous cell carcinoma patients. *Annals of oncology: official journal of the European Society for Medical Oncology / ESMO* 2013;24(12):3082-8.
30. Gabay M, Li Y, Felsher DW. MYC activation is a hallmark of cancer initiation and maintenance. *Cold Spring Harb Perspect Med.* 2014 Jun 2;4(6).
31. Schaub FX, Dhankani V, Berger AC, Trivedi M, Richardson AB, Shaw R, Zhao W, Zhang X, Ventura A, Liu Y, Ayer DE, Hurlin PJ, Cherniack AD, Eisenman RN, Bernard B, Grandori C; Cancer Genome Atlas Network. Pan-cancer Alterations of the MYC Oncogene and Its Proximal Network across the Cancer Genome Atlas. *Cell Syst.* 2018 Mar 28;6(3):282-300.
32. Bazarov AV, Adachi S, Li SF, Mateyak MK, Wei S, Sedivy JM. A modest reduction in c-myc expression has minimal effects on cell growth and apoptosis but dramatically reduces susceptibility to Ras and Raf transformation. *Cancer Res.* 2001 Feb 1;61(3):1178-86.
33. Hofmann JW, Zhao X, De Cecco M, Peterson AL, Pagliaroli L, Manivannan J, Hubbard GB, Ikeno Y, Zhang Y, Feng B, Li X, Serre T, Qi W, Van Remmen H, Miller RA, Bath KG, de Cabo R, Xu H, Neretti N, Sedivy JM. Reduced expression of MYC increases longevity and enhances healthspan. *Cell.* 2015 Jan 29;160(3):477-88.
34. Murphy DJ, Junttila MR, Pouyet L, Karnezis A, Shchors K, Bui DA, Brown-Swigart L, Johnson L, Evan GI. Distinct thresholds govern Myc's biological output in vivo. *Cancer Cell.* 2008 Dec 9;14(6):447-57.
35. Poli V, Fagnocchi L, Fasciani A, Cherubini A, Mazzoleni S, Ferrillo S, Miluzio A, Gaudioso G, Vaira V, Turdo A, Gaggianesi M, Chinnici A, Lipari E, Biciato S, Bosari S, Todaro M, Zippo A. MYC-driven epigenetic reprogramming favors the onset of tumorigenesis by inducing a stem cell-like state. *Nat Commun.* 2018 Mar 9;9(1):1024.
36. Pelengaris S, Khan M, Evan G. c-MYC: more than just a matter of life and death. *Nature reviews Cancer* 2002;2(10):764-76.
37. Field JK, Spandidos DA, Stell PM, Vaughan ED, Evan GI, Moore JP. Elevated expression of the c-myc oncoprotein correlates with poor prognosis in head and neck squamous cell carcinoma. *Oncogene* 1989;4(12):1463-8.
38. Xu B, Liu P, Li J, Lu H. c-MYC depletion potentiates cisplatin-induced apoptosis in head and neck squamous cell carcinoma: involvement of TSP-1 up-regulation. *Annals of oncology : official journal of the European Society for Medical Oncology / ESMO* 2010;21(3):670-2.
39. Waitzberg AF, Nonogaki S, Nishimoto IN, Kowalski LP, Miguel RE, Brentani RR, et al. Clinical significance of c-myc and p53 expression in head and neck squamous cell carcinomas. *Cancer detection and prevention* 2004;28(3):178-86.
40. Gera JF, Mellingerhoff IK, Shi Y, Rettig MB, Tran C, Hsu JH, Sawyers CL, Lichtenstein AK. AKT activity determines sensitivity to mammalian target of rapamycin (mTOR) inhibitors by regulating cyclin D1 and c-myc expression. *J Biol Chem.* 2004 Jan 23;279(4):2737-46.
41. Yeh E, Cunningham M, Arnold H, Chasse D, Monteith T, Ivaldi G, Hahn WC, Stukenberg PT, Shenolikar S, Uchida T, Counter CM, Nevins JR, Means AR, Sears R. A signalling pathway

- controlling c-Myc degradation that impacts oncogenic transformation of human cells. *Nat Cell Biol.* 2004 Apr;6(4):308-18.
42. Zhu J, Blenis J, Yuan J. Activation of PI3K/Akt and MAPK pathways regulates Myc-mediated transcription by phosphorylating and promoting the degradation of Mad1. *Proc Natl Acad Sci U S A.* 2008 May 6;105(18):6584-9.
  43. Lynch M, Fitzgerald C, Johnston KA, Wang S, Schmidt EV. Activated eIF4E-binding protein slows G1 progression and blocks transformation by c-myc without inhibiting cell growth. *J Biol Chem.* 2004 Jan 30;279(5):3327-39.
  44. Vander Broek R, Mohan S, Eytan DF, Chen Z, Van Waes C. The PI3K/Akt/mTOR axis in head and neck cancer: functions, aberrations, cross-talk, and therapies. *Oral Dis.* 2015;21(7):815–25.
  45. Cancer Genome Atlas Network. Comprehensive genomic characterization of head and neck squamous cell carcinomas. *Nature.* 2015 Jan 29;517(7536):576-82.
  46. Jung K 2018 Targeting phosphoinositide 3-kinase (PI3K) in head and neck squamous cell carcinoma (HNSCC)
  47. Furet P, Guagnano V, Fairhurst RA, Imbach-Weese P, Bruce I, Knapp M, et al. Discovery of NVP-BYL719 a potent and selective phosphatidylinositol-3 kinase alpha inhibitor selected for clinical evaluation. *Bioorg Med Chem Lett.* 2013;23(13):3741–8.
  48. Dejan Juric, et al Phosphatidylinositol 3-Kinase  $\alpha$ -Selective Inhibition With BYL719 (BYL719) in PIK3CA-Altered Solid Tumors: Results From the First-in-Human Study. *J Clin Oncol.* 2018 May 1; 36(13): 1291–1299.
  49. Stratikopoulos EE, Dendy M, Szabolcs M, Khaykin AJ, Lefebvre C, Zhou MM, Parsons R. Kinase and BET Inhibitors Together Clamp Inhibition of PI3K Signaling and Overcome Resistance to Therapy. *Cancer Cell.* 2015 Jun 8;27(6):837-51.
  50. Marcotte R, Sayad A, Brown KR, Sanchez-Garcia F, Reimand J, Haider M, Virtanen C, Bradner JE, Bader GD, Mills GB, Pe'er D, Moffat J, Neel BG. Functional Genomic Landscape of Human Breast Cancer Drivers, Vulnerabilities, and Resistance. *Cell.* 2016 Jan 14;164(1-2):293-309.
  51. Kurimchak AM, Shelton C, Duncan KE, Johnson KJ, Brown J, O'Brien S, Gabbasov R, Fink LS, Li Y, Lounsbury N, Abou-Gharbia M, Childers WE, Connolly DC, Chernoff J, Peterson JR, Duncan JS. Resistance to BET Bromodomain Inhibitors Is Mediated by Kinome Reprogramming in Ovarian Cancer. *Cell Rep.* 2016 Aug 2;16(5):1273-1286.
  52. Manni I, Caretti G, Artuso S, Gurtner A, Emiliozzi V, Sacchi A, et al. Posttranslational regulation of NF-YA modulates NF-Y transcriptional activity. *Molecular biology of the cell.* 2008; 19: 5203-13
  53. Bijnsdorp IV, Giovannetti E, Peters GJ. Analysis of drug interactions. *Methods Mol Biol.* 2011; 731: 421-34
  54. Bolger AM, Lohse M, Usadel B. Trimmomatic: a flexible trimmer for Illumina sequence data. *Bioinformatics.* 2014 Aug 1;30(15):2114-20. doi:10.1093/bioinformatics/btu170. Epub 2014 Apr 1. PubMed PMID: 24695404; PubMed Central PMCID: PMC4103590.
  55. Trapnell C, Pachter L, Salzberg SL. TopHat: discovering splice junctions with RNA-Seq. *Bioinformatics.* 2009 May 1;25(9):1105-11. doi:10.1093/bioinformatics/btp120. Epub 2009 Mar 16. PubMed PMID: 19289445; PubMed Central PMCID: PMC2672628.
  56. Trapnell C, Roberts A, Goff L, Pertea G, Kim D, Kelley DR, Pimentel H, Salzberg SL, Rinn JL, Pachter L. Differential gene and transcript expression analysis of RNA-seq experiments with TopHat and Cufflinks. *Nat Protoc.* 2012 Mar 1;7(3):562-78. doi: 10.1038/nprot.2012.016. Erratum in: *Nat Protoc.* 2014 Oct;9(10):2513. PubMed PMID: 22383036; PubMed Central PMCID: PMC3334321.
  57. Anders S, Pyl PT, Huber W. HTSeq—a Python framework to work with high-throughput sequencing data. *Bioinformatics.* 2015 Jan 15; 31(2): 166-9
  58. Li H, Handsaker B, Wysoker A, Fennell T, Ruan J, Homer N, Marth G, Abecasis G, Durbin R; 1000 Genome Project Data Processing Subgroup. The Sequence Alignment/Map format and SAMtools. *Bioinformatics.* 2009 Aug 15;25(16):2078-9. doi: 10.1093/bioinformatics/btp352. Epub 2009 Jun 8. PubMed PMID: 19505943; PubMed Central PMCID: PMC2723002.
  59. Robinson MD, McCarthy DJ, Smyth GK. edgeR: a Bioconductor package for differential expression analysis of digital gene expression data. *Bioinformatics.* 2010 Jan 1;26(1):139-40. doi: 10.1093/bioinformatics/btp616. Epub 2009 Nov 11. PubMed PMID: 19910308; PubMed Central PMCID: PMC2796818.

60. Irizarry RA, Hobbs B, Collin F, Beazer-Barclay YD, Antonellis KJ, Scherf U, Speed TP. Exploration, normalization, and summaries of high-density oligonucleotide array probe level data. *Biostatistics*. 2003 Apr;4(2):249-64. PubMed PMID: 12925520.
61. Adorno M, Cordenonsi M, Montagner M, Dupont S, Wong C, Hann B, Solari A, Bobisse S, Rondina MB, Guzzardo V, Parenti AR, Rosato A, Bicciato S, Balmain A, Piccolo S. A Mutant-p53/Smad complex opposes p63 to empower TGFbeta-induced metastasis. *Cell*. 2009 Apr 3;137(1):87-98. doi: 10.1016/j.cell.2009.01.039. PubMed PMID: 19345189.
62. Subramanian A, Tamayo P, Mootha VK, Mukherjee S, Ebert BL, Gillette MA, Paulovich A, Pomeroy SL, Golub TR, Lander ES, Mesirov JP. Gene set enrichment analysis: a knowledge-based approach for interpreting genome-wide expression profiles. *Proc Natl Acad Sci U S A*. 2005 Oct 25;102(43):15545-50. Epub 2005 Sep 30. PubMed PMID: 16199517; PubMed Central PMCID: PMC1239896.
63. Liberzon A, Subramanian A, Pinchback R, Thorvaldsdóttir H, Tamayo P, Mesirov JP. Molecular signatures database (MSigDB) 3.0. *Bioinformatics*. 2011 Jun 15;27(12):1739-40. doi: 10.1093/bioinformatics/btr260. Epub 2011 May 5. PubMed PMID: 21546393; PubMed Central PMCID: PMC3106198.
64. Enzo E, Santinon G, Pocaterra A, Aragona M, Bresolin S, Forcato M, Grifoni D, Pession A, Zanconato F, Guzzo G, Bicciato S, Dupont S. Aerobic glycolysis tunes YAP/TAZ transcriptional activity. *EMBO J*. 2015 May 12;34(10):1349-70.
65. Ruicci KM, Meens J, Sun RX, Rizzo G, Pinto N, Yoo J, Fung K, MacNeil D, Mymryk JS, Barrett JW, Boutros PC, Ailles L, Nichols AC. A controlled trial of HNSCC patient-derived xenografts reveals broad efficacy of PI3K $\alpha$  inhibition in controlling tumor growth. *Int J Cancer*. 2018 Nov 23.
66. Verduci L, Ferraiuolo M, Sacconi A, Ganci F, Vitale J, Colombo T, Paci P, Strano S, Macino G, Rajewsky N, Blandino G. The oncogenic role of circPVT1 in head and neck squamous cell carcinoma is mediated through the mutant p53/YAP/TEAD transcription-competent complex. *Genome Biol*. 2017 Dec 20;18(1):237.
67. Meister KS, Godse NR, Khan NI, Hedberg ML, Kemp C, Kulkarni S, Alvarado D, LaVallee T, Kim S, Grandis JR, Duvvuri U. HER3 targeting potentiates growth suppressive effects of the PI3K inhibitor BYL719 in pre-clinical models of head and neck squamous cell carcinoma. *Sci Rep*. 2019 Jun 24;9(1):9130.
68. Elkabets M, Pazarentzos E, Juric D, Sheng Q, Pelosof RA, Brook S, Benzaken AO, Rodon J, Morse N, Yan JJ, Liu M, Das R, Chen Y, Tam A, Wang H, Liang J, Gurski JM, Kerr DA, Rosell R, Teixidó C, Huang A, Ghossein RA, Rosen N, Bivona TG, Scaltriti M, Baselga J. AXL mediates resistance to PI3K $\alpha$  inhibition by activating the EGFR/PKC/mTOR axis in head and neck and esophageal squamous cell carcinomas. *Cancer Cell*. 2015 Apr 13;27(4):533-46.
69. Mizrahi A, Shamay Y, Shah J, Brook S, Soong J, Rajasekhar VK, Humm JL, Healey JH, Powell SN, Baselga J, Heller DA, Haimovitz-Friedman A, Scaltriti M. Tumour-specific PI3K inhibition via nanoparticle-targeted delivery in head and neck squamous cell carcinoma. *Nat Commun*. 2017 Feb 13;8:14292.
70. Ruicci KM, Pinto N, Khan MI, Yoo J, Fung K, MacNeil D, Mymryk JS, Barrett JW, Nichols AC. ERK-TSC2 signalling in constitutively-active HRAS mutant HNSCC cells promotes resistance to PI3K inhibition. *Oral Oncol*. 2018 Sep;84:95-103.
71. Iorio F, Knijnenburg TA, Vis DJ, Bignell GR, Menden MP et al., A Landscape of Pharmacogenomic Interactions in Cancer. *Cell*. 2016 Jul 28;166(3):740-754.

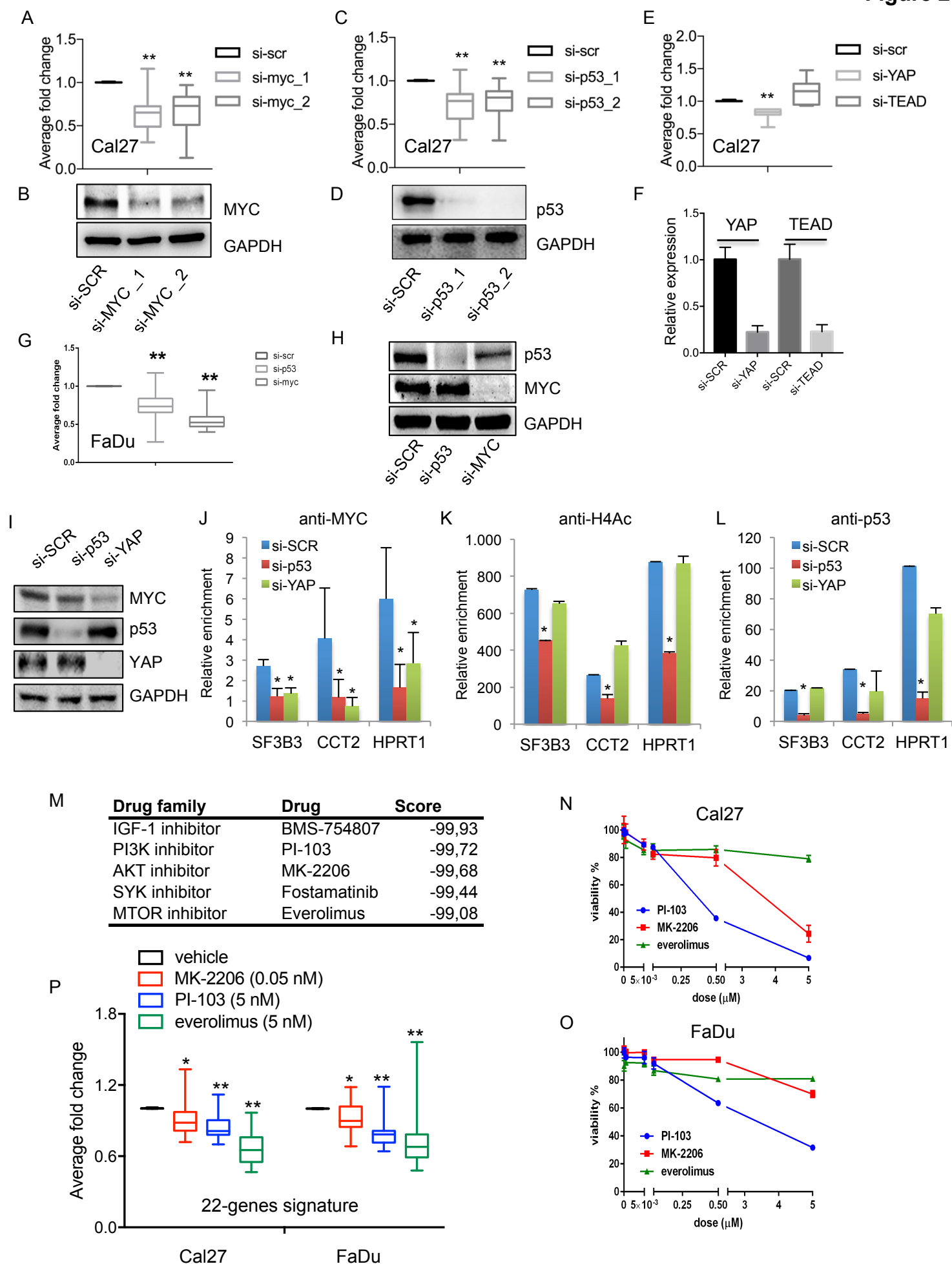


### Figure 1

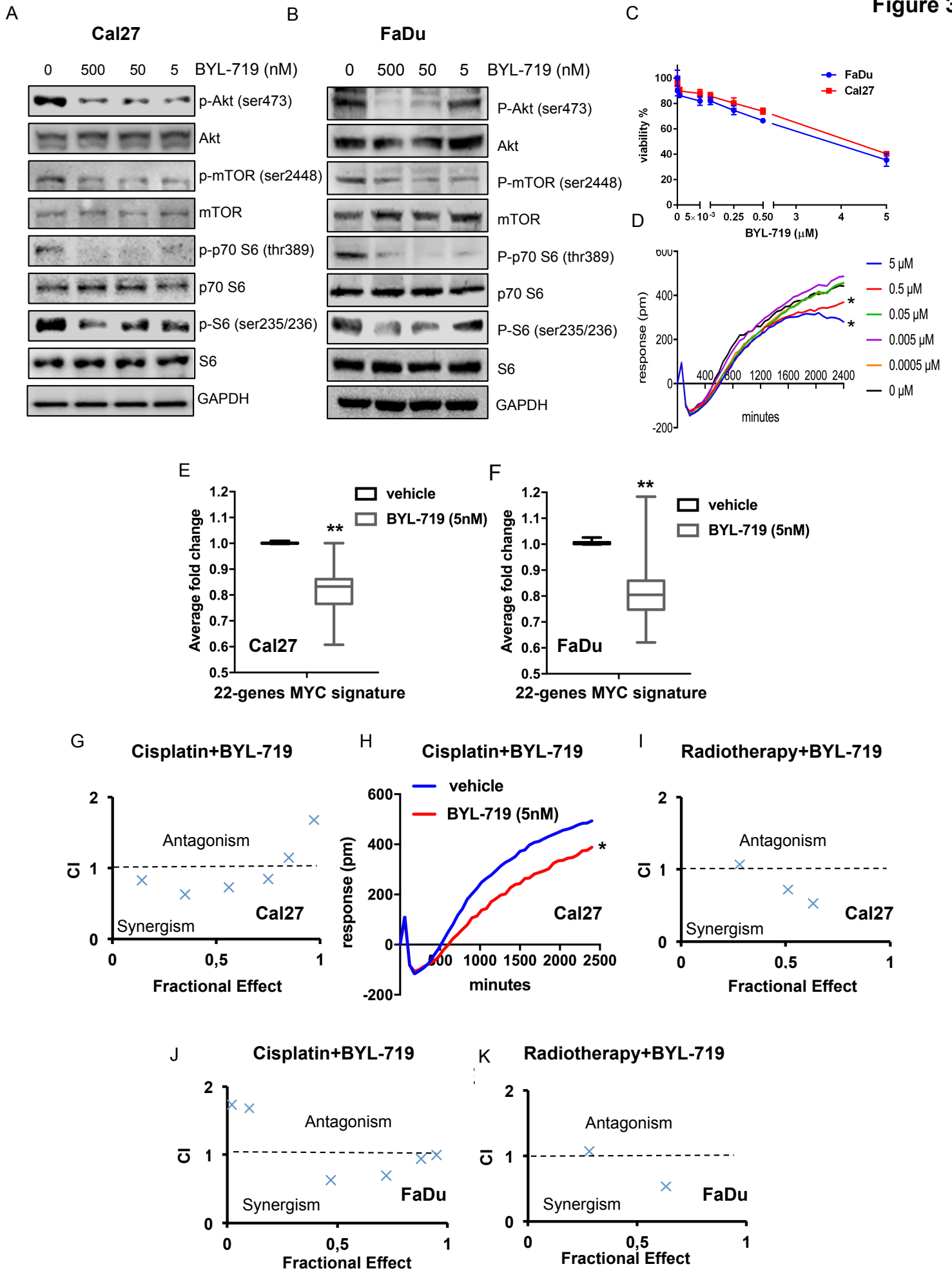


**Figure 1: Identification of a prognostic mutant p53-dependent and HNSCC-specific 22-genes MYC signature.** (A-C) Dot plot of the gene sets obtained by Preranked Gene Set Enrichment Analysis (GSEA). (A) Gene sets activated (normalized enrichment score NES>0) in TCGA-HNSCC tumors carrying a missense TP53 mutation vs. wt-p53 tumors; (B) Gene sets activated (normalized enrichment score NES>0) in HNSCC cell lines carrying a missense TP53 mutation (N=16) vs. wt-p53 (N=6) cell lines; (C) Gene sets deactivated (normalized enrichment score NES<0) in si-mutp53 vs. control si-scr Cal27 cells. Dot color indicates statistical significance of the enrichment; dot size represents the fraction of genes composing the core enrichment of gene set. Gene sets are ranked in increasing order based on the NES value. FDR: false discovery rate; NES: normalized enrichment score. (D) Z-scores heatmap of differentially expressed mRNAs after depletion of mt-p53 in Cal27 cells (RNAseq). The mutant p53-dependent signature, composed of genes down-regulated by si-p53 in Cal27 (Supplementary Table 1), has a significantly higher expression in TCGA-HNSCC tumors (n=202) carrying missense mutation in *TP53* as compared to wild-type *TP53* samples (E; \*\*\*\*p<0.0001). High level of mutp53-sig is associated with poor outcome in TCGA-HNSCC tumors (F). (G). MYC-dependent genes associated with TP53 status specifically in HNSCC were identified starting from the MYC target gene set of the MSigDB Collection and selecting a subgroup of 81 MYC-dependent genes whose mRNAs were positively correlated to MYC mRNA in both IRE (Ganci et al, 2017) and TCGA (Nature 2015) HNSCC cohorts. This 81-genes list was further merged with the p53-signature obtained from Cal27 cells, obtaining a 22-genes mutant p53-associated, HNSCC-specific MYC signature (G). The 22-genes MYC signature discriminates wt-p53-carrying tumors (WT) from those with TP53 missense mutations in TCGA HNSCCs cohort (H) and predicts survival (I).

**Figure 2**



**Figure 2: MYC and mutant p53 directly control the expression of the 22-genes signature.** A-E) RT-qPCR (A, C, E, G) analysis of the 22 genes MYC signature in Cal27 and FaDu cells depleted or not of MYC (A, G), mutant p53 (C, G), YAP or TEAD (E). Western blot (B, D, H) and RT-qPCR (F) analyses were used to assess the depletion of the indicated proteins and transcripts after transfection of siRNAs. I) Western blot analysis showing MYC, p53 and YAP protein levels in Cal27 cells interfered for the indicated proteins and used for ChIP analysis. (J-L) Chromatin Immunoprecipitation (ChIP) analysis performed on Cal27 cells depleted or not of mutant p53 or YAP expression using antibodies directed against MYC (J), H4Ac (K) and p53 (L). M) Potential inhibitors of the 22-gene MYC signature expression levels obtained combining compounds identified by Connectivity Map and information from clinicaltrial.gov. N-O) Evaluation of sensitivity of Cal27 (N) and FaDu (O) cells to the selected molecular drugs at different doses. The cell viability has been evaluated by ATPlite assay. P) Box plot representing the expression of the 22-genes MYC signature in Cal27 and FaDu cells treated with low dose of MK-2206, PI-103 or Everolimus.

**Figure 3**

**Figure 3: Low-dose BYL719 treatment affects 22-genes MYC-mp53 signature expression and sensitivity to conventional treatments in Cal27 and FaDu cells.** A, B) Western Blotting showing the effect of BYL719 treatment at the indicated doses on components of the AKT/mTOR pathway in Cal27 (A) and FaDu (B) cells. C) Evaluation of the sensitivity to PI3K inhibitor BYL719 at different doses in Cal27 and FaDu cells using ATPlite assay. D) Graph indicating the change in impedance of Cal27 cells treated BYL719 at the indicated doses for 0–2400 minutes to evaluate early changes in cell fitness. E-F) Box plot representing the expression of the 22-genes MYC signature after treatment with 5nM BYL719 for 24h in Cal27 (E) and FaDu (F) cells. G-H) Ability of BYL719 to synergize with cisplatin (CDDP), evaluated by analyzing cell viability through ATPlite assay in Cal27 (G) and FaDu (J) cells and by analyzing the change in impedance for 0–2400 minutes to evaluate early changes in cell fitness (CDDP 8  $\mu$ M) in Cal27 cells (H). (I, K) Ability of BYL719 to synergize with radiotherapy in Cal27 (I) and FaDu (K) cells by the evaluation of cell viability using ATPlite assay. (\*p<0.05, \*\*p<0.001).

Figure 4

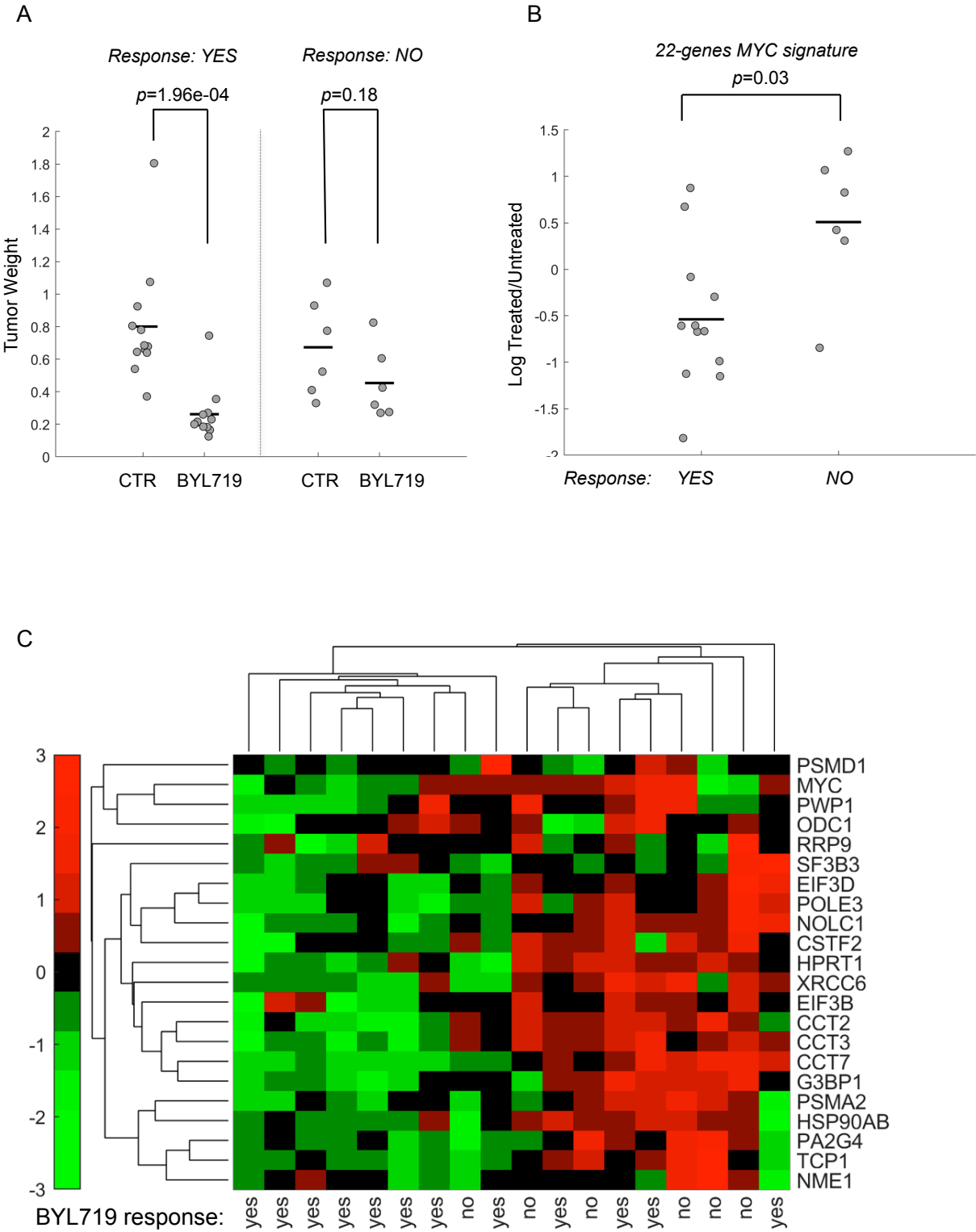


***Figure 4: Downregulation of 22-genes MYC-mp53 signature correlates with response to BYL719 in PDX models of HNSCC.*** A) Box plot showing tumor weight in PDX mouse models of HNSCC responsive (left) and not responsive (right) to BYL719 treatment. Response details in this PDX models cohort have been previously reported in Ruicci et al., 2018 (65). B) 22-genes MYC-mp53 signature in BYL719-treated vs. untreated tumors, evaluated by RT-qPCR in the groups of responsive and not responsive PDX tumors. C) Unsupervised hierarchical clustering of responsive and not responsive HNSCC PDX models based on the expression of the 22-genes MYC-mp53 signature in BYL719-treated vs. untreated tumors.



**Figure 5**

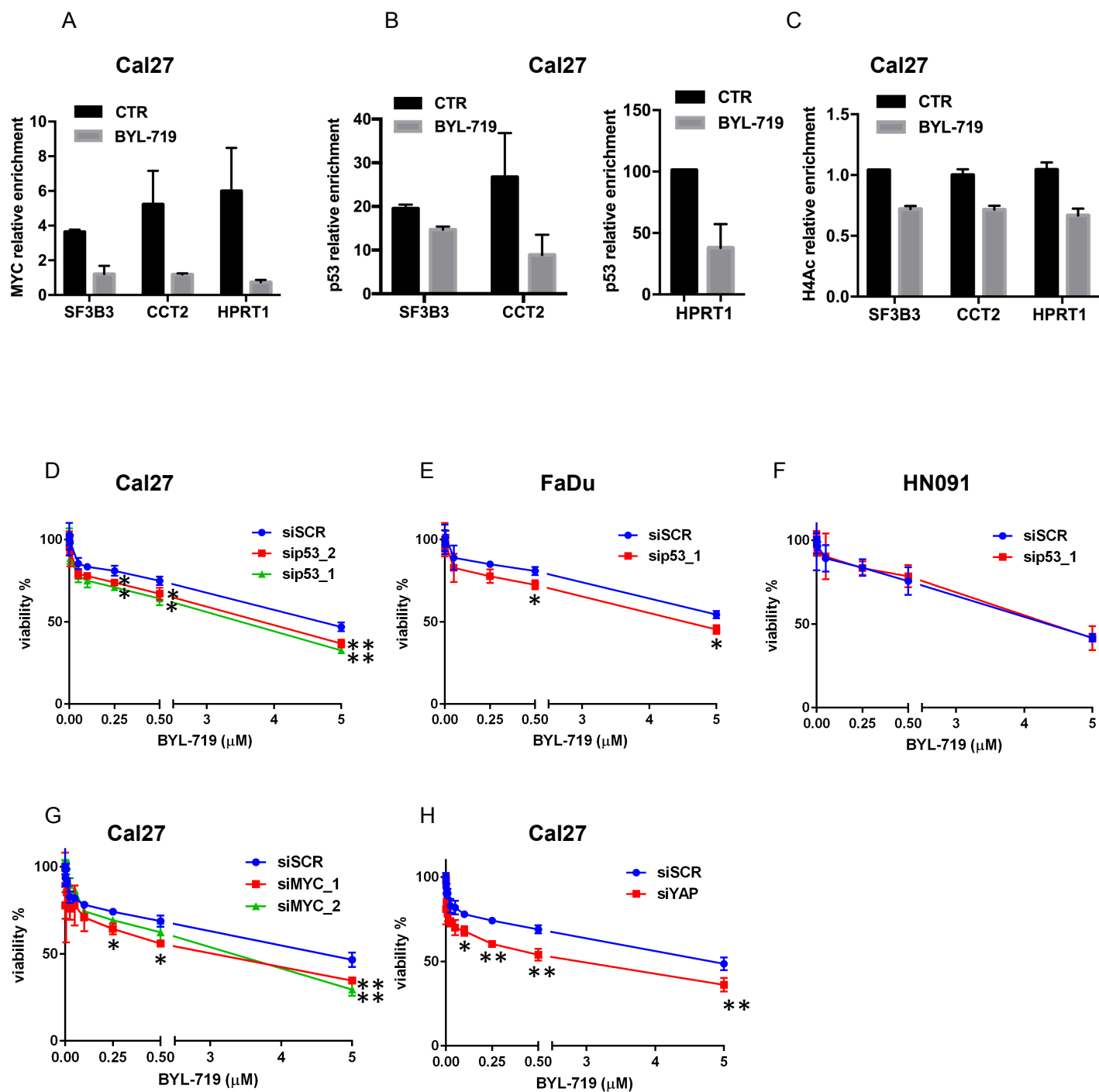


***Figure 5: Low-dose BYL719 treatment disrupts binding of MYC and mutant p53 to MYC target promoters.*** A-C) ChIP analysis of Cal27 cells treated or not with 5nM BYL719 using antibodies directed to MYC (A), p53 (B) or acetylated histone H4 (C). D-F) Dose-response curve of Cal27 (D), FaDu (E) and HN091 (F) cells transfected with siRNAs directed to p53 and subsequently treated with increasing amounts of BYL719. Viability was evaluated using ATPlite assay. G-H) Dose-response curve of Cal27 cells transfected with siRNAs directed to MYC (G) or YAP (H) and subsequently treated with increasing amounts of BYL719. Viability was evaluated using ATPlite assay.

Figure 6

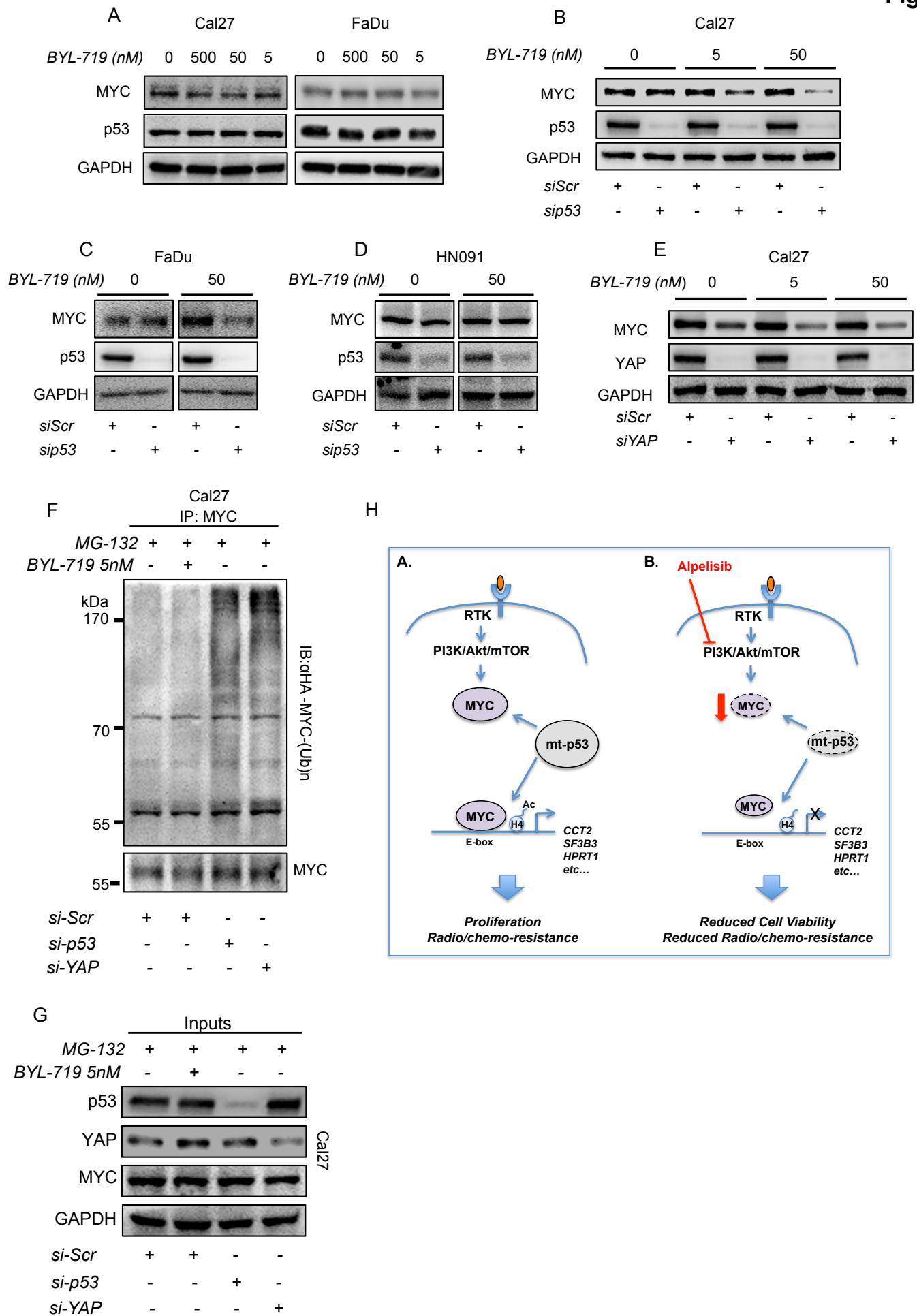


**Figure 6: Mutant p53 stabilizes MYC protein in presence of BYL719.** A) MYC and mutant p53 protein levels evaluated by Western blot in Cal27 and FaDu cells treated with increasing amounts of BYL719. B-D) Western blot analysis of the indicated proteins in Cal27 (B), FaDu (C) and HN091 (D) cells depleted or not of p53 expression and subsequently treated with the indicated doses of BYL719 for 24h. E) MYC protein levels evaluated by Western blot in Cal27 cells depleted of YAP and subsequently treated with the indicated doses of BYL719 for 24h.

F-G) Ubiquitination of MYC protein was evaluated by immunoprecipitation of MYC followed by anti-HA western blot in Cal27 cells transfected with an HA-tagged Ubiquitin expression vector. Cells treated or not with 5nM BYL719 and depleted or not of mutant p53 or YAP were analyzed. MG-132 was added to culture medium to inhibit proteasome-dependent degradation.

H) Mutant p53/MYC blocking as potential tool for the enhancement of PI3K inhibitors response. The presence of mutant p53 protein in HNSCC cells activates MYC-dependent gene expression by promoting MYC protein stability and favoring interaction of MYC with target promoters, finally leading to cell proliferation and resistance to anticancer agents (left panel, A). Inhibition of PI3K signaling and blocking of mutant p53 by RNAi lead to decreased interaction of MYC with its target promoters and to reduced levels of MYC protein, with consequent reduced cell viability and increased sensitivity to anticancer agents (right panel, B).